JOURNAL OF GEOPHYSICAL RESEARCH, VOL. 111, D23S62, doi:10.1029/2006JD007540, 2006



# Establishing Lagrangian connections between observations within air masses crossing the Atlantic during the International Consortium for Atmospheric Research on Transport and Transformation experiment

J. Methven,[1] S. R. Arnold,[2] A. Stohl,[3] M. J. Evans,[2] M. Avery,[4] K. Law,[5] A. C. Lewis,[6] P. S. Monks,[7] D. D. Parrish,[8] C. E. Reeves,[9] H. Schlager,[10] E. Atlas,[11] D. R. Blake,[12] H. Coe,[13] J. Crosier,[13] F. M. Flocke,[14] J. S. Holloway,[8] J. R. Hopkins,[6] J. McQuaid,[2] R. Purvis,[15] B. Rappenglück,[16] H. B. Singh,[17] N. M. Watson,[6] L. K. Whalley,[18] and P. I. Williams[13]

Received 30 May 2006; revised 15 September 2006; accepted 18 October 2006; published 2 December 2006.

[1] The ITCT-Lagrangian-2K4 (Intercontinental Transport and Chemical Transformation) experiment was conceived with an aim to quantify the effects of photochemistry and mixing on the transformation of air masses in the free troposphere away from emissions. To this end, attempts were made to intercept and sample air masses several times during their journey across the North Atlantic using four aircraft based in New Hampshire (USA), Faial (Azores) and Creil (France). This article begins by describing forecasts from two Lagrangian models that were used to direct the aircraft into target air masses. A novel technique then identifies Lagrangian matches between flight segments. Two independent searches are conducted: for Lagrangian model matches and for pairs of whole air samples with matching hydrocarbon fingerprints. The information is filtered further by searching for matching hydrocarbon samples that are linked by matching trajectories. The quality of these ''coincident matches'' is assessed using temperature, humidity and tracer observations. The technique pulls out five clear Lagrangian cases covering a variety of situations and these are examined in detail. The matching trajectories and hydrocarbon fingerprints are shown, and the downwind minus upwind differences in tracers are discussed.

**Citation:** Methven, J., et al. (2006), Establishing Lagrangian connections between observations within air masses crossing the Atlantic during the International Consortium for Atmospheric Research on Transport and Transformation experiment, *J. Geophys. Res.*, *111*, D23S62, doi:10.1029/2006JD007540.

## 1. Introduction to the ITCT-Lagrangian-2K4 Experiment

### 1.1. Why Was a Lagrangian Experiment Needed?

[2] Simulations of global atmospheric composition, designed to investigate climate change and air quality issues, rely on numerical models of transport and photochemistry. However, the chemical component of such models is uncertain, not only because its parameters are uncertain but also because chemical reaction mechanisms are reduced to make the problem tractable. Observations along a single flight are insufficient to evaluate the chemistry model because uncertainties in the origins of air masses dominate the uncertainty in modeled composition

[1]Department of Meteorology, University of Reading, Reading, UK.
[2]School of Earth and Environment, University of Leeds, Leeds, UK.
[3]Norwegian Institute for Air Research, Kjeller, Norway.
[4]NASA Langley Research Center, Hampton, Virginia, USA.
[5]Service d'Aéronomie, Centre National de la Recherche Scientifique, Université Pierre et Marie Curie, Paris, France.
[6]Department of Chemistry, University of York, York, UK.
[7]Department of Chemistry, University of Leicester, Leicester, UK.
[8]Earth System Research Laboratory, NOAA, Boulder, Colorado, USA.
[9]School of Environmental Sciences, University of East Anglia, Norwich, UK.
[10]Deutsches Zentrum für Luft- und Raumfahrt, Oberpfaffenhofen, Germany.
[11]Rosenstiel School of Marine and Atmospheric Science, University of Miami, Miami, Florida, USA.
[12]Department of Chemistry, University of California, Irvine, California, USA.
[13]School of Earth, Atmospheric and Environmental Sciences, University of Manchester, Manchester, UK.
[14]Atmospheric Chemistry Division, National Center for Atmospheric Research, Boulder, Colorado, USA.
[15]Facility for Airborne Atmospheric Measurements, Cranfield, UK.
[16]Institute of Meteorology and Climate Research, Forschungszentrum Karlsruhe, Garmisch-Partenkirchen, Germany.
[17]NASA Ames Research Center, Moffett Field, California, USA.
[18]School of Chemistry, University of Leeds, Leeds, UK.


0148-0227/06/2006JD007540$09.00

[*Methven et al.*, 2003]. This motivated the ambitious ITCT-Lagrangian-2K4 (Intercontinental Transport and Chemical Transformation) experiment which was a part of ICARTT (International Consortium for Atmospheric Research on Transport and Transformation) (see overview by *Fehsenfeld et al.* [2006]). Its aim was to track polluted air masses and intercept them several times as they crossed the Atlantic, time for observable photochemical transformation and mixing of air masses without experiencing further emissions.

[3] A few Lagrangian experiments have been conducted previously. Notably, the Atlantic Stratocumulus Transition Experiment (ASTEX [*Huebert et al.*, 1996]) and Aerosol Characterisation Experiments (ACE-1 [*Bates et al.*, 1998] and ACE-2 [*Raes et al.*, 2000]) measured changes in aerosol properties following air masses within the marine boundary layer. Three Lagrangian cases were observed during ACE-2 [*Johnson et al.*, 2000]. Air masses were tracked from near Portugal toward the Canary Islands using ''smart'' balloons traveling at constant altitude within the boundary layer. The physical and chemical properties of the surrounding air mass were intensively measured using the UK C-130 aircraft by intercepting the location of the balloon on three consecutive 9 hour flights (separated by only 3 hours), using forecast trajectories to determine the search area. The air masses were followed for 30 hours in each case. *Hoell et al.* [2000] conducted a timescale analysis for the first and second ACE-2 Lagrangian cases and found that meteorological effects (boundary layer entrainment and surface wind speed) and physical aerosol-cloud interactions had greatest influence over the aerosol size distribution and number concentration and that the experiment timescale was far too short for detecting chemical processing effects. In the third ACE-2 Lagrangian case the aerosol size distribution barely changed over 30 hours. *Fitzgerald et al.* [1998] estimated using a model that the evolution of aerosol from continental to marine air mass characteristics takes 6–8 days.

[4] In the stratosphere, measurements from different balloon profiles have been linked using model trajectories [*Rex et al.*, 1998; *Lehmann et al.*, 2005] and ozonesonde launches have also been timed using trajectory forecasts to achieve Lagrangian matches. Such experiments can be described as ''pseudo-Lagrangian'' since an air mass is not tracked using a physical marker drifting with the wind (such as a balloon or tracer release), but observations are linked by trajectories derived using analyzed wind fields. The quality of the Lagrangian links depends on the accuracy of the trajectory calculations and the closeness of sample points to the linking trajectories. A match is acceptable if the inferred changes in ozone concentration following the air mass exceed the measurement errors and the ''net match errors.'' *Lehmann et al.* [2005] showed that for the Match ozonesonde studies the net match errors are of similar magnitude to the measurement errors.

[5] The ITCT-Lagrangian-2K4 experiment was carried out under the auspices of IGAC. It was the first experiment aiming to take measurements that were linked by trajectories over intercontinental distances through the free troposphere, where vertical motion is important. In the main, it can be described as a ''pseudo-Lagrangian experiment'' in that the ''true trajectories'' of air parcels will never be known. *Stohl et al.* [2004] have established such a Lagrangian link between measurements across the Atlantic during September 1997 between a flight of the NOAA (National Oceanic and Atmospheric Administration) WP-3D aircraft north from Newfoundland and a flight of the UK Meteorological Research Flight C-130 west of the Azores. In this case, the upwind aircraft was not deliberately aimed at targets forecast to be Lagrangian opportunities, although both aircraft were flying at the same time as part of the North Atlantic Regional Experiment (NARE) 97. The trajectories from the actual flight track of the WP-3D were also not forecast and therefore the link was somewhat fortuitous. The ITCT-Lagrangian-2K4 aimed to maximize the chances for obtaining such links by forecasting Lagrangian opportunities and planning the flights on the basis of this information.

[6] In addition, smart balloons were released into pollution plumes leaving the New England coast on a number of occasions and the surrounding air was sampled using aircraft over an interval of several days crossing the Gulf of Maine. *Riddle et al.* [2006] show that analyzed trajectories usually follow the balloon tracks very closely, constituting a true Lagrangian experiment over a longer timescale than in ACE-2 [*Johnson et al.*, 2000].

### 1.2. Forecasting and Flight Coordination

[7] During summer 2004, there was unprecedented coverage from observational platforms measuring atmospheric constituents, including measurements from aircraft, land-based sites and a ship and a new generation of satellite platforms [*Fehsenfeld et al.*, 2006]. ICARTT formed an umbrella coordinating projects, each with differing objectives. ICARTT took advantage of this synergy by planning and executing a series of coordinated experiments to study aerosol and ozone precursors close to emissions and their subsequent chemical transformations and removal during transport. A key aim was to intercept a polluted air mass several times during its transit from North America across the Atlantic to investigate its chemical evolution in detail.

[8] Four aircraft participated actively in the ITCT-Lagrangian-2K4 experiment: the NOAA WP-3D, NASA (National Aeronautics and Space Administration) DC8, FAAM (Facility for Airborne Atmospheric Measurements) BAe146 and DLR (Deutsches Zentrum für Luft- und Raumfahrt) Falcon. There were two NOAA projects as part of ICARTT: ITCT (Intercontinental Transport and Chemical Transformation) and NEAQS (New England Air Quality Study). The NASA project was INTEX-NA (Intercontinental Chemical Transport Experiment–North America). The British and German/French projects were both named ITOP (Intercontinental Transport of Ozone and Precursors).

[9] Detailed forecasts of air mass trajectories from the east coast USA were used to identify target air masses that would pass within range of the aircraft bases in Pease (New Hampshire, USA [43.09°N, 70.83°W]), Faial (Azores [38.52°N, 28.73°W]) and Creil (France [49.25°N, 2.51°E]). The two American aircraft (hereafter WP-3D and DC8) were directed through the targets by nudging flight plans associated with the other objectives of ICARTT [*Fehsenfeld et al.*, 2006] to optimize the chance of air mass interception several days downwind. The forecasts were then refined by repeatedly calculating forward trajectories and Lagrangian plume calculations from their flight tracks

(see section 2) as the meteorological forecasts were updated. The primary goal of the two downwind aircraft (BAe146 and Falcon) was to intercept air that had been sampled close to North America.

[10] Many chemical transport models were run in forecast mode for ICARTT. However, the detailed location of targets, identified as Lagrangian opportunities, relied on the two Lagrangian models that will be discussed in section 2.

### 1.3. Establishing Lagrangian Links

[11] This paper aims to identify successful Lagrangian links between aircraft observations and to infer the changes between upwind and downwind observations for the best Lagrangian cases. Following papers will examine the chemical and physical processes responsible for the changes by using Lagrangian models running along the matching trajectories. Matches are defined as occasions when a pair of whole air samples collected during different flights (WAS-pair) exhibit highly correlated hydrocarbon fingerprints and the sample time windows are also connected by trajectories (calculated from meteorological analyses). The quality of the matches is evaluated using a third independent set of information: measurements of temperature and humidity combined into a single variable, the long-lived tracer equivalent potential temperature ($\theta_e$). The statistics of ozone and carbon monoxide differences between upwind and downwind observations are presented.

[12] *Fehsenfeld et al.* [2006] summarize the instruments and measurement techniques for observations utilized in this paper. Some salient results of the intercomparison flights are given in section 3 since these must be taken into account when estimating the uncertainty in chemical transformation inferred from upwind and downwind flights.

[13] Section 4 explains the techniques used to identify matches using Lagrangian models and hydrocarbon fingerprints. Both sets of information are then used to infer coincident matches. The quality of the matches is assessed in section 5 using probability density functions (PDFs) of the difference in observed tracer values upwind and downwind.

[14] Section 6 analyzes the best five Lagrangian cases from the ITCT-Lagrangian-2K4 experiment. The linking trajectories are shown, followed by their hydrocarbon fingerprints, composition and the inferred transformation between flights intercepting the air mass. The conclusions are presented in section 7.

## 2. Lagrangian Model Forecasts

[15] The essential processes represented in chemical/aerosol transport models are emissions, deposition, photochemical/microphysical transformation within air masses, transport of constituents by the winds and mixing between air masses by turbulence and convection. Above the boundary layer and outside regions of deep convection, the mixing timescale is generally much slower than advection timescales associated with stretching and folding of air masses by the large-scale winds (for fuller discussion see *Methven et al.* [2003]). A trace chemical is long-lived if its photochemical timescale is long compared to the advection timescales. Consequently, air masses with distinct tracer composition are stretched forming filaments on horizontal surfaces or layers on vertical profiles, with strong gradients in constituents at their edges [*Haynes and Anglade*, 1997].

[16] Air masses rapidly become too narrow to resolve in global Eulerian models where the rate of change in concentration is considered at fixed grid points. This makes it difficult to compare the model simulations with observations and also implies much too great a mixing rate which can impact the chemical transformation if the reactions are nonlinearly dependent on concentration [e.g., *Esler et al.*, 2004]. However, advection, mixing and transformation can be partitioned in different ways. Lagrangian trajectory models (section 2.1) calculate the paths of air masses (often referred to as ''particles'' because they are assumed to be infinitesimally small) following the winds resolved in atmospheric analyses or forecasts. Transformation and mixing are then calculated together following trajectories. The main problem here is the lack of knowledge about the gradients between air masses and therefore mixing. Lagrangian dispersion models (section 2.2) calculate the paths of particles following the resolved winds but also including a stochastic step to represent the effects of unresolved turbulence and convection [*Stohl et al.*, 2002]. The parameterized ''random walk'' shuffles particles, each weighted with the same tracer mass, so that their sum within a volume represents the effects of advection and diffusive mixing on passive tracer concentration [*Legras et al.*, 2003]. However, then the problem is that in this model framework a concentration is not associated with individual particles and mixing cannot affect chemical transformation along trajectories.

[17] Although all three model types have their failings, both Lagrangian approaches are attractive because they deliberately partition the processes of transformation and mixing from the advection. The dynamics of the atmosphere also conspires to allow accurate simulation of tracer structures formed by advection on scales an order of magnitude finer than the resolution of the wind field [*Methven and Hoskins*, 1999]. This means that the spacing of temperature and wind observations used to construct the meteorological analysis has less impact on the simulation of trace chemicals than uncertainty about the initial composition of air masses on leaving the boundary layer upstream.

[18] The aim of the ITCT-Lagrangian-2K4 experiment was to minimize the uncertainty associated with upwind composition by sampling there. Both types of Lagrangian models were used independently to forecast the paths of target air masses and in the identification of matches. The forecasts are described in the remainder of this section.

### 2.1. Trajectory Model Forecasts

[19] The UGAMP (U.K. Universities Global Atmospheric Modelling Programme) trajectory model [*Methven*, 1997; *Methven et al.*, 2003] calculates trajectories, given wind fields and release coordinates, using a fourth-order Runge-Kutta integration method. During ICARTT, the three wind components were calculated by transforming vorticity, divergence and surface pressure from the ECMWF (European Centre for Medium-Range Weather Forecasts) global spectral model truncated to T159 resolution on 60 hybrid pressure $\eta$ levels. The truncation from operational T511 resolution has minimal impact on trajectory forecasts compared to variations with lead time. The transformation is

identical to that used internally within the spectral model and the resulting winds were found on a Gaussian grid with spacing in longitude and latitude of approximately 1.125°. The winds at trajectory coordinates are found by cubic interpolation in the vertical and linear interpolation in the horizontal and time. Forecasts and analyses were spaced by time intervals of 6 hours and the trajectory time step was 1 hour.

[20] Domain filling trajectories were calculated backward and forward 7 days from 3D grids positioned over the east coast USA and Azores, and backward only from western Europe. The ''release grid'' spacing was 0.75° in longitude, 0.50° in latitude and 25 hPa in pressure up to 200 hPa. Trajectory calculations were initiated immediately on completion of the latest ECMWF model forecast from 1200 UT. Trajectories were released from all grids at lead times of T+00, 24, 48 and 72 hours and also at lead times of 96 and 120 hours from the Azores and European grids. In total, 854144 trajectories were calculated following each daily meteorological forecast.

[21] ''Lagrangian opportunities'' were identified by selecting the subset of trajectories from each grid that were forecast to pass within range of two or three of the aircraft bases (Pease, Faial and Creil). The useful operating range of the aircraft was defined to be 1000 km. The subset was typically a small fraction of the whole set and was usually clustered into a few coherent ensembles of trajectories. Plots of all Lagrangian opportunities for a given grid and lead time (available from http://badc.nerc.ac.uk/data/itop/) were used for rapid selection of dates meriting further examination.

[22] In order to identify Lagrangian opportunities that would also be likely to be polluted, emission tracers were calculated. Gridded estimates of surface emissions were converted to volume sources by assuming instantaneous mixing throughout the depth of the boundary layer. Boundary layer depth was taken from the ECMWF model output. The sources were then integrated along trajectories whenever they were within the boundary layer. The NOx emissions inventory from the Emission Database for Global Atmospheric Research (EDGAR [*Olivier et al.*, 1999]) was used to estimate the influence of anthropogenic emissions and the isoprene emissions inventory from *Guenther et al.* [1995] was used to indicate the influence of biogenic emissions (as a monthly mean). Clearly, both of these species have short lifetimes (less than a day) so the emission tracers have much higher concentrations than could be observed along flights. Lagrangian opportunities were filtered on the basis that the anthropogenic emission tracer accumulated along back trajectories must exceed a threshold (10 ppbv) and the accumulated emissions along forward trajectories must stay below the same threshold. In this way, targets were identified with air masses leaving the continental boundary layer that would also pass within range of downwind aircraft.

[23] Figure 1 shows an example of an emission tracer forecast for the U.S. east coast domain for a verification time 1200 UT 15 July 2004, based on an ECMWF forecast starting from 1200 UT 13 July 2004. The air near points A and B was also forecast to pass within range of the Azores and Europe. The NOAA WP-3D aircraft was directed into targets A and B and the NASA DC8 also sampled air mass B on its descent into Pease.

[24] Emission tracers were also used to visualize the polluted air mass structure over the Atlantic. Typically the air masses are stretched and folded into thin, sloping sheets (e.g., Figure 13b in section 6.2.5) seen as filaments on horizontal surfaces. The forecasts were used to determine the shortest route to the target and the best level to intercept it. Then the aircraft could be directed in the along-filament direction, sampling the air mass at several altitudes.

[25] The target location was refined further by calculating trajectories forward from the actual flight track of the upwind aircraft. The coordinates were made available for the calculation within hours of landing. Trajectories were released every 10 s along the tracks. The main displacement errors in trajectories are in the along-filament direction [*Methven and Hoskins*, 1999] so by flying through the forecast location of the target filament it is likely that air of similar composition will be sampled, even if the trajectory match has a displacement of tens of kilometers in the retrospective analysis.

[26] Clearly, the forecast trajectories from flight tracks varied as the wind forecasts were updated, but qualitatively the set of trajectories retained similar shapes even though the first forecasts (for example 7 days forward from T+72 hours into the meteorological forecast) are based on wind forecasts extending to very long lead times (10 days). On many occasions the targets sampled upwind drifted out of range of the downwind aircraft as the forecast lead time reduced, but in many cases the targets remained within range and were sampled (see section 6 for the best cases).

### 2.2. Lagrangian Dispersion Model Forecasts

[27] During ICARTT forecasts were also made using FLEXPART, a Lagrangian particle dispersion model that simulates transport (by resolved winds), diffusion, dry and wet deposition. Details of the model are recorded by *Stohl et al.* [2005]. In its backward in time (retroplume) mode, FLEXPART has been shown to simulate measurements of long-lived trace constituents at ground-based sites and along aircraft tracks to the extent that potential source contributions from different regions can be determined with some confidence [*Forster et al.*, 2001; *Stohl et al.*, 2002, 2003].

[28] During the ICARTT period FLEXPART was run forward in time. About 100000 particles were released per day with locations weighted by an emission inventory such that each particle is associated with the same mass of CO on release. North American emissions were based on the point, onroad, nonroad and area sources from the U.S. EPA National Emissions Inventory (area sources at 4 km resolution) plus Mexican emissions north of 24°N and all Canadian sources south of 52°N [*Frost et al.*, 2006]. The inventories are estimates for the year 1999. Outside this domain the EDGAR emission inventory was used [*Olivier et al.*, 1999]. Particles were carried for 20 days before removal from the simulation. The positions of these particles were recorded every 2 hours. The number of particles per unit volume gives an estimate of CO concentration away from the sources. FLEXPART was driven by forecasts and analyses of winds from the Global Forecast System model of NCEP (National Center for Environmental Prediction) at $1^\circ \times 1^\circ$ resolution on 26 pressure levels with a temporal resolution of 3 hours.

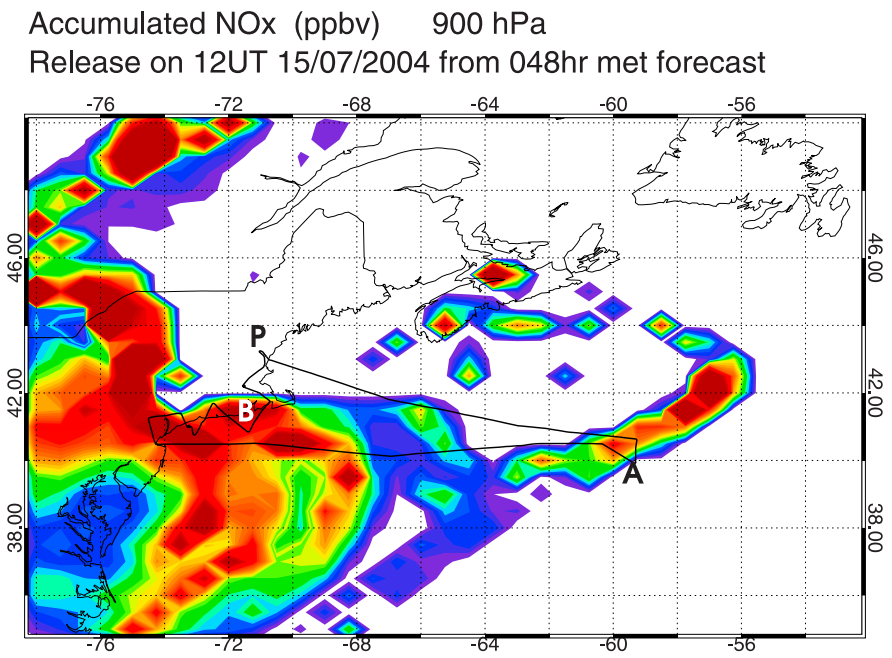


**Figure 1.** The 48 hour forecast depicting NOx emission tracer at 900 hPa in the U.S. domain for the verification time 1200 UT 15 July 2004. A and B mark Lagrangian targets identified from the forecast. The flight track of the NOAA WP-3D aircraft from Pease, New Hampshire (point P), is overlain. Contour interval is 1 ppbv.

[29] As described by *Stohl et al.* [2004], Lagrangian opportunities were sought by following these particles backward in time from the operational areas of each aircraft (Pease, Faial and Creil) and applying the following criteria: (1) The separation between the particle release point and potential upwind link must exceed 12 hours and a distance of 800 km. (2) The CO tracer mixing ratio must not decrease back in time by more than 20%. (3) The RMS separation of back trajectories released from one tracer output cell ($1^\circ \times 1^\circ \times 1000$ m) must not exceed 100 km plus 5% of travel distance. This eliminates cases with rapid back trajectory separation, indicating air being brought together from very different origins and therefore not a good candidate for a Lagrangian case study. The Lagrangian opportunities were ranked according to their CO tracer mixing ratio weighted by the number of aircraft that could possibly sample it.

[30] Once flights had taken place, particles were released from boxes of size $0.7^\circ \times 0.7^\circ \times 400$ m centered along the flight track and opportunities were ranked by measured CO.

[31] Often the FLEXPART model with its Lagrangian opportunity criteria highlighted different targets to the UGAMP trajectory model with its emissions tracer criteria, but on reinspection the same targets were identified by both models. Each group examined the forecast products that they were most familiar with: FLEXPART forecasts for the NOAA WP-3D team, the UGAMP RDF forecasts for the ITOP-UK team and both for the Falcon team. Agreement spotted during discussion lent weight to the decision to pursue a target. FLEXPART forecasts were focussed toward planning the upstream flights and were particularly useful in ruling out cases when dilution by mixing was predicted to be too great for the chemical contrast of the air mass to remain distinct.

[32] Comparison was also important because the two Lagrangian models used forecast winds from different meteorological centers (primarily for reasons of data access) which could introduce differences in target locations of several hundred km on the European side of the Atlantic, especially at long lead times. The differences were used to indicate robustness in forecast Lagrangian opportunities.

[33] It will be shown in section 5 that both models result in a similar quality of coincident matches, although there are many cases where only one of the models identifies a match due to the very strict, but differing, selection criteria. In the matching analysis FLEXPART was also driven by ECMWF analyses.

## 3. Airborne Measurements

[34] The instruments on the four aircraft participating in the ITCT-Lagrangian-2K4 experiment and the characteristics of their measurements are summarized by *Fehsenfeld et al.* [2006].

[35] In order to infer changes in chemical composition following air masses, it was crucial to compare the measurements by the different aircraft flying in formation as close together as possible. Three comparison flights were made between the WP-3D and DC8 on 22 July, 31 July and 7 August. The DC8 and BAe146 made a rendezvous over the mid-Atlantic on 28 July. Two comparison flights were made between the BAe146 and Falcon: over England on 7 July and over France on 3 August.

[36] The ozone comparison is of particular interest since it provides estimates of the limits on the determination of the net ozone production imposed by measurement uncertainty. During each of six comparison flights the ozone measurements were well correlated and exhibited only small sys-

tematic differences. The results indicate that the average ozone measurements agree within ±2 ppbv and the 1-sigma precision of the 1-s average data is better than ≈ 1 ppbv [*Fehsenfeld et al.*, 2006].

[37] For CO, the comparison between the DC8 and BAe146 was hindered by the lack of data from the fast response LARC DACOM instrument on the DC8 on 28 July. However, whole air samples on the DC-8 were analyzed for CO to provide a comparison with the BAe146 on 28 July and with the fast response CO data on the other DC-8 flights throughout the ICARTT campaign. The results indicate that the average CO measurements agree within ±3 ppbv for the DC-8, WP-3D and DLR Falcon, but are biased low by 4 ppbv on the BAe146. The 1-sigma precision of the 1-s average data is better than ≈2 ppbv on all four aircraft.

[38] Ambient air samples were circulated to the laboratories of the different groups associated with each aircraft. The hydrocarbon measurements were highly consistent [*Lewis et al.*, 2006]. It was difficult to compare whole air samples from comparison flights because of the different sampling times and variability within the air masses. However, it is clear that the hydrocarbon fingerprints of samples taken within one air mass are very similar (typically the statistic defined by equation (2), $r > 0.9$).

[39] The frequency of data recorded by instruments varies a great deal. Throughout this paper all data are shown with 10 s resolution. Higher-frequency data have been averaged over 10 s windows centered on the time stamp. Lower-frequency data (e.g., whole air samples) are repeated at every time point throughout the sample interval. Data from all instruments on the DC8 and BAe146 aircraft were collated in this way into "data merges" for each flight.

## 4. Search for Lagrangian Matches

### 4.1. Trajectory Model Matches

[40] Trajectories were released at 10 s intervals from flight tracks and integrated forward and backward so that all the associated "air masses" were followed over the same 35 day time interval (1200 UT 1 July 2004 to 5 August 2004). The four ITCT-Lagrangian-2K4 aircraft made 40 flights during the period of opportunity (6 July 2004 to 1 August 2004 plus the flights of the BAe146 and Falcon on 3 August), requiring 91901 trajectories from flight tracks. A time point on a flight was labeled as a match if its associated trajectory shadowed a trajectory from another flight over the time window between the flights. If the flights were separated by less than 4 days, the comparison time window is extended to 4 days centered on the midtime between the flights. The criteria for "shadowing" was taken to be a mean difference in latitude and equivalent potential temperature ($\theta_e$) of less than 0.5° and 2 K respectively, averaged over the trajectory time window. For the comparison, $\theta_e$ was interpolated from the ECMWF analyses to points spaced at 6 hour intervals along the trajectories. Note that often the magnitude of change in (analyzed) $\theta_e$ following a trajectory over the time window is much greater than 2 K (e.g., associated with mixing or radiative cooling) but a similar evolution must occur for both trajectories in a matching pair such that their average separation is less than 2 K.

[41] In principal the match criteria based on two variables alone could allow erroneous matches where a pair of trajectories followed the same history of latitude and $\theta_e$ but at different longitudes or altitudes. However, not a single case occurred out of the $4.1 \times 10^9$ trajectory pairs, indicating that there is negligible chance for trajectories to shadow each other this closely over a 4 day window unless they are within neighboring air masses.

[42] A single trajectory from flight A may "match" with many trajectories from flight B. Conversely, any one of those matching trajectories from flight B may match with many other trajectories from flight A ("converse matches"). The many-many relationship is complex, even if only one distinct air mass links the flights, because the two flights will have spent different times within the air mass and may have intersected it on several occasions. No trajectory from flight A matches a trajectory from flight B exactly. The complexity is reduced by selecting the "best" matching trajectory from flight B for every time point along flight A. The definition of best is also problematic. One could choose the match with the smallest latitudinal separation for example. However, this may select air masses that were sampled for a very brief time. The chosen method was to select the trajectory from flight B that has the most converse matches with flight A. In this way the "best match trajectories" are the most representative of a coherent ensemble of trajectories that match both flights. These trajectory-only (best) matches are marked by color bars on the time series shown in Figure 2a. Considering all ITCT-Lagrangian-2K4 flights there are 30887 best matching pairs.

### 4.2. FLEXPART Model Matches

[43] CO tracers were simulated by running the Lagrangian dispersion model FLEXPART forward in time as for the forecasts (section 2.2). The flight tracks were divided into segments with intervals of 0.2 degrees from horizontal flight legs (or whenever the aircraft altitude changed by more than 50 m below 300 m, 150 m below 1000 m, 200 m below 3000 m or 400 m above this). All particles located within 30 km horizontally and 200 m vertically of a segment were identified and traced forward for a maximum of 10.5 days. The centroid position of these particles and their standard deviation about the centroid was calculated. The North American CO tracer was determined at all particle positions and averaged over those from each flight segment.

[44] Matches were defined on the basis of the same criteria used for the identification of Lagrangian opportunities, but with different trajectory separation criteria. The horizontal distance between the plume centroid trajectory and downwind measurement point plus the plume standard deviation must be less than 18% of the distance traveled. The vertical separation between the plume centroid trajectory and a measurement plus the standard deviation must be less than 1000 m plus 0.02% of the horizontal distance traveled.

[45] In total, 395 FLEXPART "Lagrangian cases" were identified and ranked according to the distance criteria above. By the time a plume has reached the mid-Atlantic these two criteria are generally less strict than the trajectory match criteria (latitude separation < 0.5° and $\theta_e$ separation < 2 K). Some of these cases involved more than two aircraft flights and these were given greater weight in the ranking.

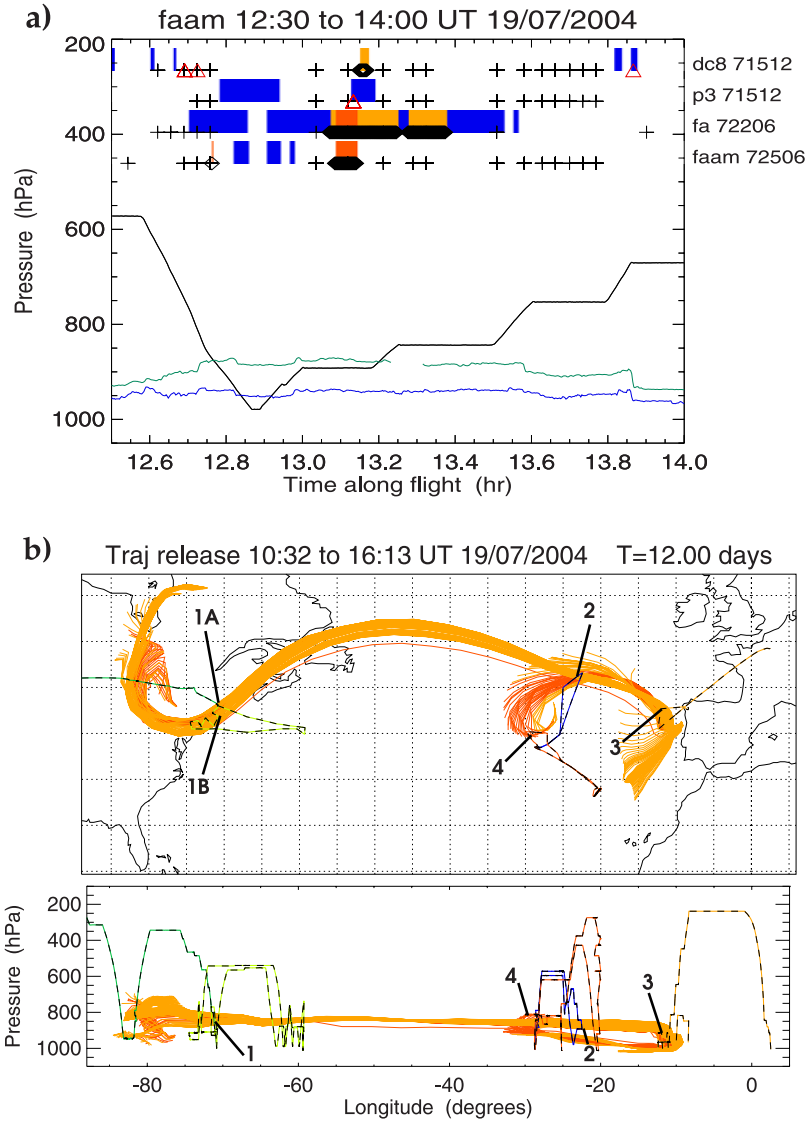


**Figure 2.** (a) Lagrangian matches shown versus time along the flight of the BAe146 aircraft on 19 July 2004. The black line shows pressure (hPa). The green and blue lines show CO and ozone using the *y* axis (1000-C) where C is volume mixing ratio in ppbv. Matches are shown with four other flights: DC8 on 15 July, WP-3D on 15 July, Falcon on 22 July and BAe146 on 25 July. Crosses mark matching hydrocarbon samples. Blue color bars indicate times with trajectory-only matches. Coincident matches are colored and marked by diamonds. Red triangles mark FLEXPART matches. (b) Trajectories 6 days backward and forward from the flight track on 19 July (blue) that shadow trajectories from the other flights shown and also link air samples with similar hydrocarbon fingerprints ("coincident matches"). Matching flights are DC8 15 July (dark green), WP-3D 15 July (light green), Falcon 22 July (orange) and BAe146 25 July (red). Lagrangian interceptions are numbered in time order.

In total there were 489 matches between flight time segments. These are marked by red triangles in Figure 2a.

[46] Although far fewer FLEXPART matches are depicted than trajectory matches, in section 4.4 it will be shown that a similar number of coincident matches are pulled out by both models. This is because a much higher fraction of FLEXPART matches are coincident matches. Also many trajectory matches (up to 200) can be linked to one hydrocarbon match and only the best is indicated as the "coincident match."

### 4.3. Hydrocarbon Fingerprinting

[47] Multicomponent hydrocarbon measurements provide a means for distinguishing air masses because their relative amounts are variable. In addition, photochemical ageing can be inferred from compounds with a range of different lifetimes with respect to OH reaction [e.g., *Jobson et al.*, 1998]. If a polluted air mass mixes with a clean background, containing almost zero hydrocarbon concentrations, then the ratio of any two hydrocarbons only evolves because of their different photochemical loss rates. Problems with comparing absolute concentrations from upwind and downwind

samples of an air mass with variable concentrations, but distinct composition, are to some extent circumvented by considering ratios.

[48] *Parrish* [2006] examines the difficulties in using hydrocarbon ratios to infer age of air (since leaving the source region) that arise because air masses mix with others that are not clean and have different fingerprints because they have experienced different sources. The distribution of sources can be estimated using the footprint of a retroplume calculation using a Lagrangian dispersion model. It is typically found that when following a retroplume backward in time it spreads slowly until close to the boundary layer. Here, it will be assumed that the upwind measurements are taken above the boundary layer and that little mixing occurs before the downwind measurements. Under these assumptions, upwind and downwind air samples can be described as having the same composition if their fingerprints of hydrocarbon ratios match, after accounting for the evolution associated with OH loss. A. Arnold et al. (Statistical inference of OH concentrations and air mass dilution rates from successive observations of non-methane hydrocarbons in single air masses, submitted to *Journal of Geophysical Research*, 2006, hereinafter referred to as Arnold et al., submitted manuscript, 2006) infer the mixing rate averaged along trajectories in addition to the OH concentration by assuming different backgrounds, estimated from the observations.

[49] Hydrocarbon fingerprints were compared between all pairs of "whole air samples" (WAS pairs) collected by the four aircraft. Matches were identified in the following way.

[50] 1. The concentration ratio, $h_i$, of 7 hydrocarbons to ethane is found for upwind and downwind flights (to factor out dilution by mixing to a clean background). The hydrocarbons used in order of increasing reactivity with OH are: acetylene, propane, benzene, iso-butane, n-butane, pentane and hexane ($i$ = 1,..,7).

[51] 2. The upwind ratios are adjusted to account for photochemical loss between measurement times by taking logs and using the rate coefficients for OH reaction, $k_i$, assuming a constant OH concentration:

$$y_i = \ln(h_i(t_1)) - (k_i - k_{ethane})[OH](t_2 - t_1) \quad (1)$$

where $t_1$ and $t_2$ are the upwind and downwind sample times, and $y_i$ is described as the "adjusted upwind ratio."

[52] 3. For each WAS pair the scatter plot of downwind and adjusted upwind ratios is compared with the 1:1 line and closeness of fit measured with the statistic:

$$r = 1 - \frac{\sqrt{\frac{1}{N-1}\sum \frac{1}{2}(y_i - x_i)^2}}{X} \quad (2)$$

where $x_i = \ln(h_i(t_2))$ and $X$ exceeds the maximum range of $x$ values in the data ($X$ = 6). Note that the closest point on $x = y$ to a measurement pair $(x_i, y_i)$ is $x = y = \frac{1}{2}(x_i + y_i)$ separated by the distance-squared $\frac{1}{2}(y_i - x_i)^2$. Therefore the quantity $1 - r$ equals the RMS deviation from the line $x = y$ divided by the range in the data. $N$ is the number of hydrocarbons (in addition to ethane) measured in common on both flights (cases where $N < 3$ were rejected).

[53] 4. The pair is labeled a "WAS match" if $r$ exceeds the 90th percentile obtained using all WAS pairs from that pair of aircraft.

[54] 5. The matching procedure was repeated for varying OH to find the concentration that gave the highest value for $r$ at the 50th and 90th percentiles. It was found that the identification of Lagrangian matches is quite insensitive to variations in OH in the range 0 to $4 \times 10^6$ molec cm$^{-3}$ because the longest-lived compounds are barely affected by the OH adjustment. A concentration of $2 \times 10^6$ molec cm$^{-3}$ was used to define WAS matches. The trans-Atlantic matches are most sensitive because of the long time elapsed between samples. Arnold et al. (submitted manuscript, 2006) infer similar OH concentrations using a more rigorous method for each Lagrangian case (see section 6) allowing for mixing and taking into account measurement uncertainties and observed variability within air masses. The OH value is consistent with global estimates by *Prinn et al.* [1995].

[55] In total there are 239608 matches meeting the fingerprint criteria. However, most of the WAS matches between samples collected by the DC8 and the WP-3D are not linked by trajectories but simply reflect the degree of similarity between air masses over the east coast USA, close to the emissions. When DC8-DC8, P3-P3 and DC8-P3 matches are excluded, the number of matches reduces to 50582. WAS matches are marked by crosses on the time series in Figure 2a.

### 4.4. Coincident Matches

[56] A search was made for the subset of all match trajectories that link both time segments associated with a WAS pair. Every WAS measurement was associated with a 6 min time segment in searching for linking trajectories. Samples typically take less than a minute to fill but the window was extended to allow for phase errors in the matching trajectories. These "coincident matches" are marked by the diamonds and a color bar on Figure 2a. The color corresponds with the color of the matching flight track shown in Figure 2b.

[57] All the "coincident match" trajectories from the BAe146 flight track (dark blue) on 19 July are shown in Figure 2b extending 6 days backward and 6 days forward. The coincident trajectories' colors correspond with the last flight that they intersect.

[58] Using all 40 ITCT-Lagrangian-2K4 flights, only 576 WAS matches were also linked by matching trajectories. Since the trajectories are released every 10 s from the flight tracks, there are typically many matching trajectories associated with each of these cases. These will be called "coincident match trajectories": 8847 were found between all ICARTT flights, reducing to 1276 coincident matches when those between the USA aircraft are excluded (DC8-DC8, P3-P3, DC8-P3).

[59] A similar search was made for all FLEXPART matches that link with both ends of a WAS match (called FH-linked for FLEXPART-Hydrocarbon). The time segments centered on the time stamp for WAS samples and FLEXPART matches were given a width of 6 min and the flights were divided into 10 s intervals (just as for the trajectories) for the purposes of these searches. 1974 FH-linked matches were found between all ICARTT flights,

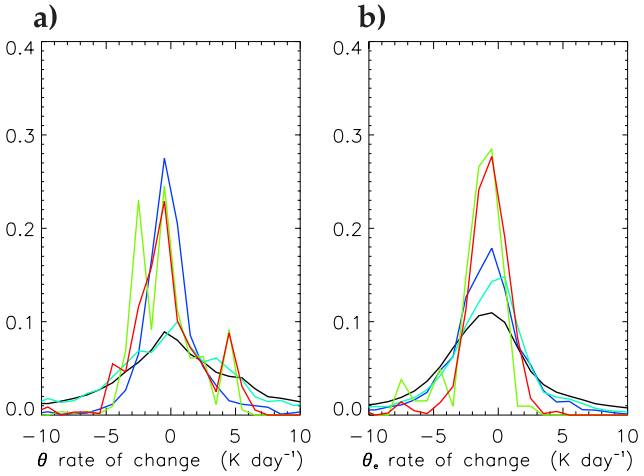


**Figure 3.** Normalized histograms showing average rate of change along match trajectories between upwind and downwind observations for (a) potential temperature and (b) equivalent potential temperature. The curves show results for different types of matches: coincident trajectory-hydrocarbon (red), FLEXPART-hydrocarbon (green), trajectory only (blue), hydrocarbons only (cyan) and random pairs of time points from matching flights (black). The bin size used was 1 K day$^{-1}$, and the sum over bins equals one for each histogram.

reducing to 527 FH-linked matches when those between the USA aircraft are excluded (DC8-DC8, P3-P3, DC8-P3).

[60] Finally, consistency between the two models and WAS matches is investigated by searching for coincident match trajectories that link with both time segments of each FLEXPART match (called CF-linked for coincident FLEXPART). All the matches and corresponding time stamps are listed at http://www.met.rdg.ac.uk/∼swrmethn/icartt. Only the best five Lagrangian cases will be discussed in section 6.

## 5. Evaluation of Matches Using Independent Tracer Observations

[61] The quality of the independent model and hydrocarbon matches and their coincident matches is assessed using further independent data sets: measurements of temperature, humidity, CO and ozone. A running median filter with a time window of 6 min was passed through all the time series of aircraft data. A running median was used (rather than running mean) because it preserves the location and gradient associated with boundaries between distinct air masses, while removing rapid fluctuations that cannot be associated with particular trajectory behavior. It has little impact on the time series far from emissions, but smooths out rapid fluctuations over the USA close to sources, especially in the boundary layer. The filtered aircraft data is interpolated to the release points used for the trajectories (at 10 s intervals). Differences between upwind and downwind potential temperature ($\theta$), equivalent potential temperature ($\theta_e$), CO and ozone are calculated for every match. PDFs of these differences are plotted for the various methods: trajectory matches, WAS matches, coincident matches and FH-linked matches.

[62] The potential temperature difference between downwind and upwind samples is divided by their time separation to give the average rate of change following air masses. The resulting PDF (Figure 3a) is strongly peaked on slow cooling (0 to −2 K day$^{-1}$) for coincident trajectory-hydrocarbon matches and a similar PDF is obtained using FLEXPART-hydrocarbon (FH-linked) matches. This value is consistent with constant radiative cooling under clear skies. The trajectory-only matches are also strongly peaked near zero, indicating that most of the trajectories that match are almost isentropic. In contrast, the PDF for WAS matches is much flatter indicating that many samples with similar hydrocarbon fingerprints are not within the same air mass (i.e., not linked by trajectories).

[63] Note that the black curve was obtained by selecting $n$ time points at random from the time series of two flights and using observed $\theta$ from these pairs of points to calculate $(\theta_2 - \theta_1)/(t_2 - t_1)$. Each pair of flights was weighted by setting $n$ equal to the number of trajectory matches between them. The "random" histogram illustrates the similarity of the air masses sampled on flights that are linked, irrespective of Lagrangian connections. Therefore its values cannot be interpreted as heating rates following air masses. The identification of Lagrangian matches is only successful if the PDF for matches is more strongly peaked than the PDF for randomly selected time points. Clearly, WAS matches alone are not significantly different from random selection.

[64] Note that the coincident and FH-linked PDFs have a secondary peak at a heating rate of about 5 K day$^{-1}$. This can be attributed to the time-averaged rate of latent heat release in ascending air masses. A better thermodynamic tracer of air masses is equivalent potential temperature, $\theta_e$, that is conserved for the pseudoadiabatic process of a saturated air mass experiencing condensation. The PDFs for rate of change of $\theta_e$ (Figure 3b) are even more strongly peaked on weak cooling for coincident and FH-linked matches. Trajectory-only matches are clearly not as good as coincident matches. $\theta_e$ reveals that although trajectory matches may occur in the same isentropic layer (range of $\theta$ values) they can have the wrong specific humidity for a Lagrangian match. The additional requirement for a hydrocarbon match pulls out the matches with similar humidity. Conversely, the PDF for WAS matches is more peaked for $\theta_e$ than for $\theta$. This shows that the $\theta_e$ signature and hydrocarbon fingerprint are correlated, both being indicative of air mass origin, even if two samples are not linked by trajectories.

[65] Upwind and downwind matching observations are used to estimate "growth rates" for Figure 4 using:

$$\sigma_c = \frac{1}{t_2 - t_1}(\ln C_2 - \ln C_1) \tag{3}$$

[66] Photochemical loss of CO via OH reaction would result in $\sigma_c \approx -0.018$ day$^{-1}$, assuming an OH concentration of $2 \times 10^6$ molec cm$^{-3}$. The effects of CO loss were detected in the North Atlantic Regional Experiment [*Parrish et al.*, 1998]. However, since the photochemical lifetime is much longer than the typical mixing timescale, mixing is expected to dominate CO changes following an air mass. Mixing with a uniform dilute "background" would result in

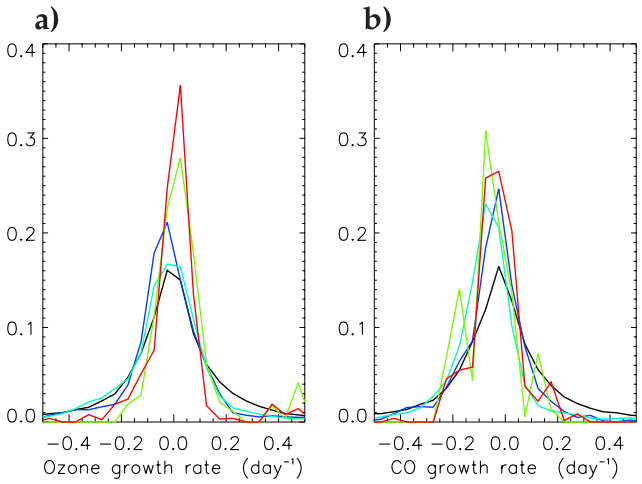


**Figure 4.** Normalized histograms showing average growth rate along match trajectories between upwind and downwind observations for (a) ozone and (b) carbon monoxide. Lines are colored as in Figure 3. The bin size is 0.05 day$^{-1}$.

exponential decay of concentration with timescale $-1/\sigma_c$. However, typically pollution plumes do not have much higher CO concentrations than their surroundings, since CO is rather long-lived, and dilution of CO within the center of the plume will be slow even if turbulent mixing is active. In this case, $-1/\sigma_c$ cannot be interpreted as a turbulent mixing timescale. The narrow PDF peak for "CO growth rate" occurs between 0 and $-0.1$ day$^{-1}$, indicative of a slow dilution timescale exceeding 10 days. Weak CO increase is inferred from some match pairs. This is most likely to result from a slight mismatch in a plume with high variability. For example the downwind flight may have crossed the maximum plume concentration while the upwind aircraft may have sampled only the flanks or flown just above or below the air mass sampled downstream.

[67] The "ozone growth rate" PDF for coincident matches peaks just above zero, consistent with slow photochemistry and mixing. The positive peak is perhaps attributable to net photochemical ozone production in the polluted Lagrangian matches. Stronger decrease and increase is seen for a few matches. Photochemical modeling effort to explain the observations will be focussed on the best Lagrangian cases described in the next section.

## 6. Best ITCT-Lagrangian-2K4 Cases

### 6.1. Observed Hydrocarbon Fingerprints

[68] Overall, the matching methods agree that there were five main Lagrangian cases, each linking at least three flights across the Atlantic. The Lagrangian cases were identified on the basis of coincident matches where samples with similar hydrocarbon fingerprints are linked by matching trajectories and/or FLEXPART model matches. Figure 5 shows the hydrocarbon fingerprints from all the flights linked in each case. For each sample, ratios of hydrocarbons relative to ethane are found, $h_i$, and then these are adjusted to account for loss by reaction with OH using equation (1) to the time of the designated reference flight for that case (see last column of Table 1). The flight linked with the most other flights, or the furthest upwind was chosen as the reference. The ratios are decreased for flights occurring before the reference time and increased for flights occurring after the reference time. Note that the rate coefficients, $k_i$, have a weak temperature and pressure dependence.

[69] In the scenario of a pollution plume experiencing oxidation and mixing with a dilute (zero) background, the OH-adjusted ratios for the samples in each case should be indistinguishable. Arnold et al. (submitted manuscript, 2006) estimate the OH required to produce a best fit between the ratios and also improve the method, estimating OH from hydrocarbon concentrations allowing for mixing with a realistic background derived from the data. Cases 1A and 5 are consistent with OH between 1.5 and 3 $\times$ 10$^6$ molec cm$^{-3}$ and the value 2 $\times$ 10$^6$ molec cm$^{-3}$ has been used here. An OH concentration of 1 $\times$ 10$^6$ molec cm$^{-3}$ obtains a better fit for cases 2 and 4A. In cases 3 and 4B the best fit is obtained with zero OH and some ratios are slightly higher downstream. This indicates that the Lagrangian match is not perfect and the elevated downstream ratios are thought to arise from mixing within the pollution plume between interceptions. Nevertheless, the spread between linked samples is much less than randomly selected samples and also much less than the variability between species, although the spread between samples increases with reactivity. Therefore each case has a distinct hydrocarbon fingerprint and the linked flights did indeed sample almost the same air mass.

[70] The fingerprint in case 2 differs markedly from the others and is particularly elevated in benzene and ethene (ethene is not shown for the other cases because its concentration downstream is close to the detection limit). Case 2 sampled a plume from forest fires in Alaska, while the other cases sampled anthropogenic pollution. Note that the last flight (green) in case 5 is elevated in benzene/ethane relative to its matches and it is argued in the next section that this results from mixing with a layer of fire emissions above. A similar explanation could account for the high benzene/ethane for the last flight of case 1A where the DLR Falcon observed an Alaskan fire plume directly above the target air mass.

### 6.2. Composition Change Inferred From Lagrangian Cases

[71] The tracer characteristics observed during the time windows linked by the Lagrangian cases are shown in Table 1. The mean and standard deviation has been calculated using 1 s data over the time windows. The number of whole air samples collected during each window is also indicated.

[72] The penultimate column shows the peroxy acetylnitrate (PAN) concentration measured by the DC8, WP-3D and BAe146. Where DC8 measurements of PAN by the PANAK instrument (H. B. Singh et al., Reactive nitrogen distribution and partitioning in the North American troposphere and lowermost stratosphere, submitted to *Journal of Geophysical Research*, 2006) are missing, the higher-frequency TD-LIF measurements for the sum of peroxy nitrates (PNs) are shown [*Day et al.*, 2002]. Note that PNs is dominated by PAN. The Falcon did not measure PAN, but total reactive nitrogen ($NO_y$) was measured. The DC8 and WP-3D also measured $NO_y$ but the BAe146 $NO_y$ measurement unfortunately did not produce

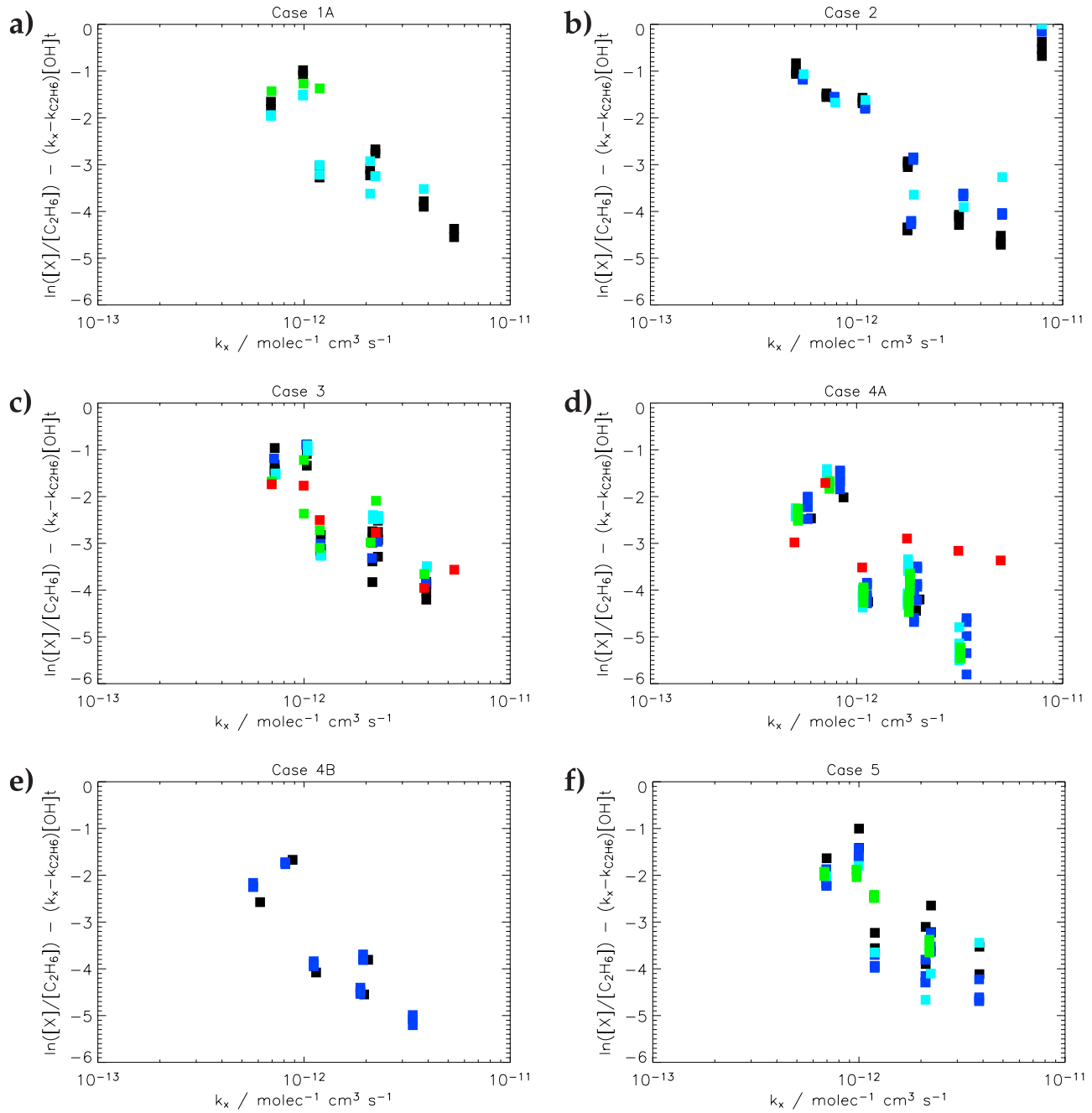


**Figure 5.** (a–f) Ratios of hydrocarbon concentrations to ethane, adjusted for loss by reaction with OH, plotted against the rate coefficient, $k_x$. In order of increasing $k_x$ the species are acetylene, propane, benzene, iso-butane, *n*-butane, pentane, hexane and ethene (case 2 only). The OH varies between cases to demonstrate best fit (see text). The flights in each case are colored in time order as shown in Table 1: black, 1; dark blue, 2; pale blue, 3; green, 4; red, 5.

results during ICARTT. In the upper level cases 2 and 4, most of the $NO_y$ was in the form of PAN, while at low levels (cases 1, 3 and 5) PAN is a much smaller fraction of $NO_y$ as a result of thermal decomposition.

[73] The last column shows the "growth rate" of CO over the intervals linking each flight segment with the designated reference flight for that case. The growth rate is always calculated forward in time, such that a negative value indicates CO decrease. Most of the decrease can be attributed to mixing with more dilute neighboring air masses, since CO photochemical loss is much slower.

#### 6.2.1. Case 1: USA to Portugal

[74] Figure 2b shows the trajectories for all coincident matches with the BAe146 flight on 19 July 2004. The orange trajectories link with the Falcon on 22 July off the coast of Portugal and some of them also link with the DC8 as it descended into Pease on 15 July. The red trajectories also link with the BAe146 on 25 July as the air returned toward the Azores from close to Portugal. Both the orange

**Table 1.** Measurements Taken During Lagrangian Match Windows Defined by the Times $t_{start}$ and $t_{end}$ in Days Since 0000 UT 1 January 2004[a]

| Flight | $t_{start}$, day | $t_{end}$, day | Leg | WAS | $\theta$, K | $\theta_e$, K | CO, ppbv | $O_3$, ppbv | PAN, pptv | $\frac{\Delta(\ln[CO])}{\Delta t}$, day$^{-1}$ |
|---|---|---|---|---|---|---|---|---|---|---|
| *Case 1A*: *USA to Portugal* (*Low Level*) | | | | | | | | | | |
| 15 Jul DC8 | 197.84375 | 197.84506 | P | 2 | 299.0 (1.4) | 329.0 (1.0) | 147.4 (12.3) | 59.1 (1.7) | – | ref |
| 15 Jul WP-3D | 197.87292 | 197.87875 | L | 0 | 298.7 (0.4) | 330.6 (0.7) | 166.4 (10.8) | 69.1 (1.6) | 901 (142) | – |
| 19 Jul BAe146 | 201.54081 | 201.54868 | L | 2 | 296.2 (0.5) | 321.5 (0.5) | 125.4 (2.8) | 60.5 (1.9) | 33 (15) | −0.044 (0.023) |
| 22 Jul Falcon | 204.52851 | 204.53256 | L | 1 | 295.7 (0.2) | 319.1 (0.7) | 106.0 (1.1) | 46.4 (0.7) | 400 (14)[b] | −0.049 (0.013) |
| *Case 1B*: *USA to Portugal* (*Lowest Level*) | | | | | | | | | | |
| 15 Jul DC8 | 197.84506 | 197.84771 | L | 4 | 296.9 (0.7) | 331.7 (0.3) | 183.2 (6.1) | 60.9 (4.7) | – | ref |
| 15 Jul WP-3D | 197.85916 | 197.86333 | L | 0 | 298.2 (0.5) | 332.3 (0.9) | 203.3 (6.2) | 80.2 (1.8) | 1107 (215) | – |
| 22 Jul Falcon | 204.54167 | 204.54720 | L | 1 | 293.4 (0.2) | 321.4 (1.2) | 111.4 (1.3) | 42.0 (1.0) | 470 (31)[b] | −0.074 (0.005) |
| 25 Jul BAe146 | 207.77020 | 207.77367 | L | 1 | 300.7 (0.2) | 322.8 (1.0) | 83.0 (2.9) | 32.9 (2.2) | 9 (2) | −0.080 (0.005) |
| *Case 2*: *Alaskan Fire Plume* (*Upper Level*) | | | | | | | | | | |
| 18 Jul DC8 | 200.77740 | 200.79333 | L | 3 | 319.4 (0.3) | 320.2 (0.2) | 448.7 (68.0) | 61.6 (2.6) | 2228 (413)[c] | ref |
| 20 Jul BAe146 | 202.51820 | 202.52208 | L | 3 | 319.0 (0.1) | 320.1 (0.1) | 415.4 (49.1) | 67.5 (1.2) | 2672 (296) | −0.044 (0.110) |
| 23 Jul Falcon | 205.54083 | 205.55042 | L + L | 1 | 314.0 (0.9) | 319.4 (1.4) | 242.5 (34.9) | 78.9 (3.6) | 1960 (245)[b] | −0.129 (0.044) |
| *Case 3*: *USA to Ireland* (*Low Level*) | | | | | | | | | | |
| 20 Jul WP-3D | 202.87833 | 202.89583 | L | 5 | 298.1 (0.2) | 334.1 (1.1) | 199.7 (30.1) | 90.1 (15.1) | 648 (330) | ref |
| 21 Jul WP-3D | 203.74625 | 203.75042 | L | 1 | 299.2 (0.2) | 334.1 (1.1) | 184.2 (12.3) | 89.4 (6.6) | 492 (119) | −0.093 (0.190) |
| 22 Jul WP-3D | 204.72042 | 204.72917 | P + L | 2 | 297.3 (1.2) | 333.5 (1.6) | 181.8 (7.5) | 57.2 (6.4) | 260 (68) | −0.051 (0.085) |
| 25 Jul Falcon | 207.66250 | 207.68125 | L | 4 | 294.8 (0.9) | 321.5 (2.3) | 137.5 (11.9) | 43.5 (2.9) | 175 (37)[b] | −0.078 (0.036) |
| 26 Jul Falcon | 208.71583 | 208.72222 | L | 1 | 294.5 (0.4) | 316.7 (0.6) | 121.0 (1.8) | 42.6 (1.5) | 924 (422)[b] | −0.086 (0.026) |
| *Case 4A*: *Upper Level Export by Frontal System* | | | | | | | | | | |
| 25 Jul DC8 | 207.77257 | 207.77384 | P | 1 | 315.1 (0.8) | 330.0 (2.6) | 104.4 (4.6) | 61.6 (2.4) | 292 (30)[c] | −0.003 (0.017) |
| 27 Jul WP-3D | 209.66667 | 209.69167 | L | 5 | 317.2 (0.5) | 339.7 (2.0) | 109.7 (11.6) | 64.5 (4.9) | 392 (73) | −0.032 (0.063) |
| 28 Jul DC8 | 210.78584 | 210.79626 | L | 5 | 336.4 (0.2) | 338.5 (0.2) | 113.0 (4.9) | 70.9 (3.0) | 567 (64) | −0.123 (0.088) |
| 29 Jul BAe146 | 211.51750 | 211.53125 | L + P | 5 | 334.5 (1.1) | 337.9 (1.0) | 103.3 (4.9) | 70.4 (6.0) | 572 (91) | ref |
| 31 Jul Falcon | 213.52277 | 213.52571 | P + L | 1 | 331.3 (1.0) | – | 85.3 (1.4) | 78.9 (5.4) | 663 (56)[b] | −0.095 (0.025) |
| *Case 4B*: *Upper Level Export by Frontal System* | | | | | | | | | | |
| 25 Jul DC8 | 207.75173 | 207.75289 | P | 1 | 318.6 (1.4) | 336.5 (0.6) | 106.0 (3.2) | 67.5 (5.5) | 341 (68)[c] | ref |
| 29 Jul BAe146 | 211.53343 | 211.54292 | L | 3 | 335.7 (0.5) | 338.1 (0.5) | 111.0 (2.2) | 79.9 (5.0) | 643 (33) | 0.011 (0.010) |
| *Case 5*: *Low-Level Export by Frontal System* | | | | | | | | | | |
| 27 Jul WP-3D | 209.77708 | 209.78750 | L + P | 2 | 306.1 (0.7) | 337.1 (2.4) | 124.0 (10.2) | 67.7 (3.5) | 416 (33) | ref |
| 28 Jul WP-3D | 210.83333 | 210.84583 | L | 4 | 304.6 (0.4) | 333.1 (1.7) | 98.9 (7.5) | 62.8 (3.9) | 186 (29) | −0.214 (0.107) |
| 31 Jul BAe146 | 213.48375 | 213.48917 | P | 1 | 302.0 (1.7) | 330.0 (1.0) | 94.6 (3.2) | 51.6 (3.0) | 56 (27) | −0.073 (0.024) |
| 1 Aug BAe146 | 214.48583 | 214.49167 | L | 3 | 301.8 (0.3) | 324.0 (0.7) | 97.7 (2.5) | 48.8 (3.2) | 18 (5) | −0.051 (0.018) |

[a]The flights legs are labeled P for profile or L for level, or both. The number of hydrocarbon samples is given. Data for each window are shown as "mean (standard deviation)." The last column shows the "growth rate" for CO between the flight in that row and the reference flight for the Lagrangian case.
[b]$NO_y$ is shown rather than PAN for the Falcon.
[c]PNs measurement is shown rather than PAN in some DC8 cases.

and red trajectories shadow trajectories from the WP-3D flight on 15 July (close to point B on Figure 1) but because of a system malfunction no WAS measurements were made on this half of the flight and therefore hydrocarbon fingerprints cannot be compared. However, the match with the WP-3D is also indicated by the FLEXPART model (red triangle in Figure 2a).

[75] Further examination reveals two distinct cases: coincident matches along the DC8 track occur with the BAe146 19 July at higher altitude (855 hPa) than with BAe146 25 July (902 hPa). Similarly, matches occur along the Falcon track with the BAe146 19 July at 913 hPa (orange trajectories) but with the BAe146 25 July on a lower-level run (at 965 hPa) within the marine boundary layer (red trajectories). Therefore this case has been split into two, with case 1B occurring at slightly lower altitude than case 1A. The split is confirmed by the distinct hydrocarbon fingerprints for the two cases. Case 1B is more polluted and has a higher butane/ethane ratio.

[76] In case 1A, the DC8 and WP-3D match windows were separated by less than an hour and 0.35° latitude on their descent into Pease from the west. The WP-3D was at slightly lower altitude (887 hPa compared with DC8 window average of 855 hPa) where CO and ozone were higher. PAN was not measured by the DC8 on this descent, but almost 1 ppbv was observed by the WP-3D.

[77] Another segment along the WP-3D track which has trajectory and FLEXPART matches with the Falcon and BAe146 is further south by about 100 km (near Cape Cod). It has been attributed to case 1B, although the WP-3D crossed the maximum in the plume downwind of the New York conurbation (level at 928 hPa) and clearly observed higher CO and ozone than the DC8 closer to Pease.

[78] Potential temperature varies little following the air mass 1A, but $\theta_e$ decreases, consistent with a decrease in specific humidity while maintaining constant temperature between Pease and the BAe146 on 19 July (as occurs in case 3). The CO mixing ratio decreases with time but at a surprisingly slow rate indicating a $1/\sigma_c$ timescale in the

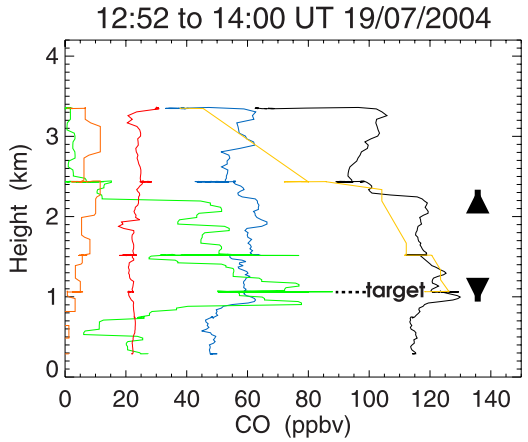


**Figure 6.** Profiles of measurements made by the BAe146 between 1252 and 1400 UT on 19 July 2004. Black indicates CO (ppbv). Blue indicates ozone (ppbv). Green indicates sulfate aerosol (0.1 × $\mu$g m$^{-3}_{STP}$). Yellow indicates ethane (0.01 × ppbv). Orange indicates PAN (0.01 × ppbv). Red indicates $\theta_e$ − 300 (K). The $y$ axis uses the pressure-height coordinate $z$ = 44330.77[1 − $(p/p_0)^{0.19026}$]m where $p_0$ = 1013.25 hPa.

range 15–25 days. Ozone is seen to decrease systematically following both air masses. Experiments (not shown here), using Lagrangian photochemical models initialized with the composition observed by the WP-3D, show that the rate of ozone decrease can be accounted for by photochemical loss in the humid air mass even without allowing for any mixing and deposition.

[79] Figure 6 shows measurements made by the BAe146 in ascent through the polluted layer (0.9 km to 2.3 km) which was oriented roughly west-east and was intercepted at the northeast extreme of the flight track [see *Lewis et al.*, 2006, Figure 9]. The highest CO, ethane and sulfate aerosol concentrations occur at the target level of 1.05 km (≈ 900 hPa) that matches the other four flights. Ozone is seen to be lower in the marine boundary layer, although still well elevated compared to clean episodes near the Azores in the same month ([$O_3$] ∼ 10–20 ppbv [see *Lewis et al.*, 2006]). There is a rapid increase in concentrations at 0.9 km, indicating that mixing is weak above the boundary layer and that this layer has not been in contact with the ocean.

[80] The extremely high level of sulfate aerosol was also observed off the east coast USA in the lower troposphere and on several other days in the Azores region (BAe146 flights on 17, 20, and 22 July). Source contributions estimated using FLEXPART in retroplume mode indicate that this originates from the coal burning power plants, especially in the Ohio River Valley and picks up further emissions approaching the east coast USA. The scenario of pollution leaving the continental boundary layer and then forming two layers over the ocean, within and above the marine boundary layer, was also observed during the third Lagrangian case in ACE-2 [*Johnson et al.*, 2000]. Entrainment from the case 1A layer into the marine BL would help oppose ozone (and sulfate aerosol) loss there (case 1B).

#### 6.2.2. Case 2: Alaskan Fire Plume

[81] Throughout July 2004, the mid to upper troposphere above North America and the Atlantic was highly perturbed by emissions from boreal forest fires in Alaska and later in Canada [*Pfister et al.*, 2005]. A number of Lagrangian links were made between flights sampling these fire plumes and case 2 is the best linked of these matches and occurred after the DC8 had sampled an intense plume near Newfoundland on 18 July (point F in Figure 7a).

[82] Figure 8a shows the flight track of the BAe146 relative to the plume on 20 July. Since air can travel 100s of km while a flight is occurring, the track coordinates have been shifted using short forward and backward trajectories to the estimated positions of sampled air masses at an instant, 1200 UT. This enables clearer comparison of the flight track with the air mass structure simulated for a single time frame using the Reverse Domain Filling trajectory technique for a 3D domain (RDF3D) [*Methven et al.*, 2003]. Back trajectories were released from the 3D grid over the Azores region. The specific humidity, $q$, from the ECMWF analyses was interpolated to the origin of every trajectory (3 days before "arrival" on the grid) and log $q$ was used to color their arrival points. The driest air (green) was strung out in a long, thin filament at the 525 hPa level, and contained the fire plume. This plume was intercepted four times: near points A, B, C and in the descent home after C. Figure 8b shows the specific humidity structure on cross section XY. The fire plume occurred within dry intrusions that had descended from close to tropopause level over North America, presumably the level that material was carried to by convection above the fires.

[83] The best trajectory match with the DC8 flight track is at point A, but unfortunately hydrocarbon samples were not measured there. However, back trajectories from point B pass just above the flight level of the DC8 through the plume at point F in Figure 7a. Three WAS measurements were made within plume B as seen for ethane on Figure 9 and these had a very high correlation with the three WAS measurements by the DC8 within the plume. CO, PAN and organic aerosol were extremely elevated within the plume, while sulfate aerosol was almost negligible.

[84] Table 1 shows that $\theta_e$ matches to within 1 K between interceptions. CO is extremely variable within the air mass, although the variability decreases with time. The timescale ($-1/\sigma_c$) of CO decrease between the DC8 and Falcon is about 8 days. In this case the plume is very concentrated relative to its surroundings, so that this can be associated with the timescale for turbulent mixing. It is consistent with an estimate from hydrocarbon fingerprints (Arnold et al., submitted manuscript, 2006).

[85] Ozone increases significantly following this air mass. L. Whalley et al. (unpublished manuscript, 2006) and *Real et al.* [2006] show that Lagrangian photochemical models initialized with the DC8 observations can account for this increase, although when mixing is parameterized the modeled ozone increase falls short.

#### 6.2.3. Case 3: USA to Ireland

[86] Another excellent example of pollutant export across the Atlantic at low levels followed the passage of a cold front across east coast USA. The WP-3D aircraft deliberately sampled air downwind of the New York urban area on 20 July and then targeted the same air on two successive days as it slowly crossed the Gulf of Maine and Nova Scotia. The DC8 flew nearby during its flights on 20 and

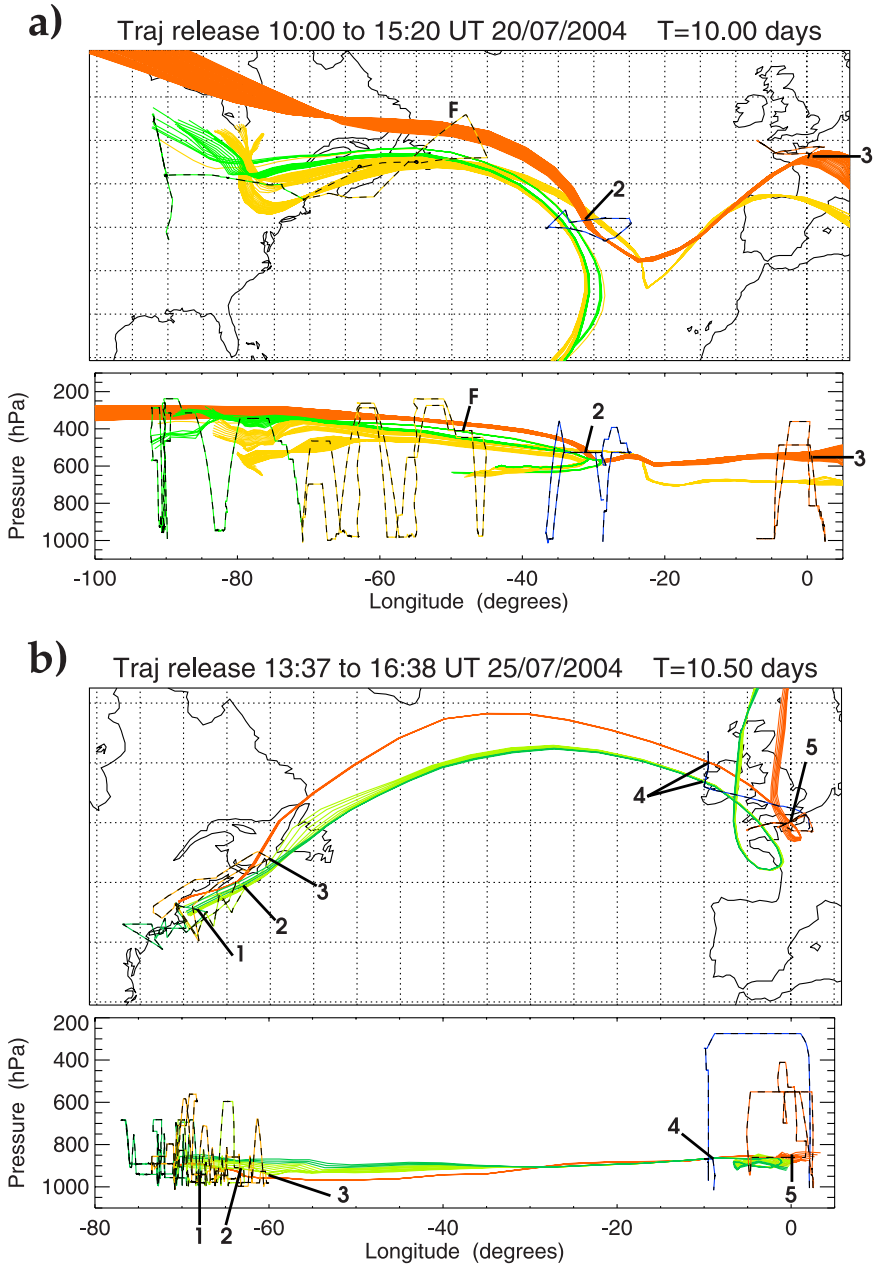


**Figure 7.** Lagrangian links between hydrocarbon samples from different flights with similar fingerprints ("coincident matches"). (a) Case 2: trajectories 5 days forward and backward from the BAe146 flight track on 20 July (blue). Matching flights are DC8 15 July (green), DC8 18 July (yellow) and Falcon 23 July (red). F marks the intersection of the Alaskan fire plume by the DC8 on 18 July. (b) Case 3: trajectories 5.25 days forward and backward from the Falcon flight track on 25 July (blue). Matching flights are WP-3D 20 July (dark green), WP-3D 21 July (light green), WP-3D 22 July (orange) and Falcon 26 July (red), labeled in time order.

22 July. Two smart balloons were also released into the pollution plume from New York and followed it across the Gulf of Maine [*Riddle et al.*, 2006].

[87] As shown in Figure 7b, the Falcon flew from France to intercept the air mass just west of Ireland on 25 July. Note that the FLEXPART matches were indicated at about 850 hPa on the initial descent of the Falcon to low levels off the Irish coast (1542 UT) but no hydrocarbon sample was taken. The coincident trajectory-hydrocarbon matches occur on the level run at 870 hPa. CO and ozone levels are very similar for these two flight segments, indicating that the matches are in essentially the same air mass. Finally, the target was forecast to cross Ireland and SW England overnight and the Falcon again intercepted it over the English Channel on 26 July.

[88] The Falcon observed higher butane/ethane ratios to the west of Ireland (green symbols in Figure 5c) than the WP-3D observed in the match windows on 20, 21 and

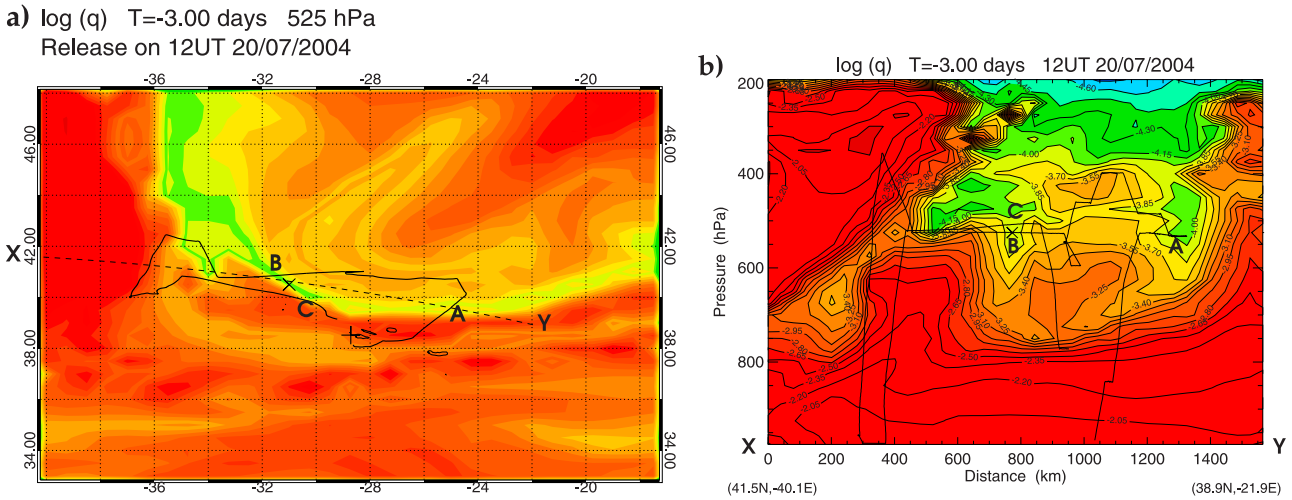


**Figure 8.** (a) RDF3D reconstruction of specific humidity on the 525 hPa surface, 1200 UT 20 July 2004. The flight track of the BAe146 is shown shifted relative to air mass locations at 1200 UT. At this level the aircraft intercepted an Alaskan fire plume at points A, B and C. The plume is colocated with a narrow filament of dry air (green). The plus symbol marks Faial. Longitude and latitude are labeled around the map. (b) Great circle cross section XY, marked by the dashed line in Figure 8a. The BAe146 flight track is projected onto the section. Color shading shows log $q$ with contour interval of 0.15.

22 July. However, the WP-3D flight on 21 July zigzagged across the pollution plume 3 times while flying toward the northeast. Much higher butane/ethane ratios were observed to the south of the matches with the Falcon (where CO$\sim$230 ppbv). The ratios indicate that mixing occurred within the plume after 22 July during transit across the Atlantic.

[89] Equivalent potential temperature decreases a great deal between the WP-3D close to Nova Scotia and the Falcon near Ireland, while $\theta$ is almost unchanged. The air mass was not intercepted over the mid-Atlantic but analyzed temperature and humidity interpolated from the ECMWF model to the trajectories indicates that humidity decreased along the entire trajectory. The WP-3D flights on 21 and 22 July observed a dry layer with lower $\theta_e$ immediately above the polluted target. Continuous entrainment from above into the polluted air mass could explain the humidity decrease while maintaining potential temperature.

[90] On 26 July the Falcon intersected the air mass over the English Channel. However, $NO_y$ was strongly elevated in a narrow spike during the match window with a large fraction in the form of short-lived $NO_x$. This spike is clearly indicative of fresh emissions, probably from southern England, and accounts for the high mean and standard deviation in $NO_y$ (Table 1). The fresh emissions also elevated the short-lived hexane content (red symbols in Figure 5c).

[91] The long-term record at Mace Head on the west coast of Ireland shows that CO as high as 100 ppbv is rare when air approaches from the west [*Derwent et al.*, 1998]. It is uncommon for large-scale plumes from the USA to travel within the lower troposphere on such a northerly trajectory. More frequently low-level export heads toward the Azores, as observed at Pico (D. Helmig, unpublished manuscript, 2006). Usually, air heading northeastward from the USA and then curving round to Europe is associated with strong ascent along the east coast USA within warm conveyor belts and the outflow crosses western Europe in the upper troposphere [*Eckhardt et al.*, 2004].

#### 6.2.4. Case 4: Upper Level Export by Frontal System

[92] Case 4 is an example of such ascent and upper level export associated with a warm conveyor belt (WCB) from SE USA along the east coast to the upper troposphere near Nova Scotia. There was also much deep convection over the eastern USA which would have carried pollutants into the upper troposphere where they could then be advected in the strong westerlies across the Atlantic.

[93] The FLEXPART model indicated a Lagrangian match between the midtroposphere over the USA sampled by the WP-3D on 27 July (marked "2" in Figure 10a) and the upper troposphere to the west of the Azores sampled by the BAe146 on 29 July. The location of this air mass, as

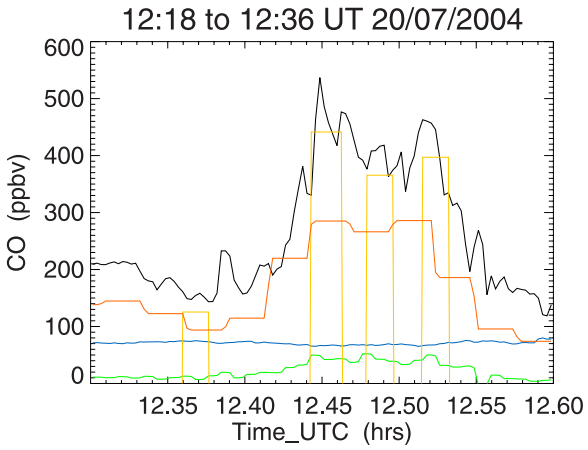


**Figure 9.** Time series of measurements made by the BAe146 through fire plume B between 1218 and 1236 UT on 20 July 2004. Black indicates CO (ppbv). Blue indicates ozone (ppbv). Green indicates organic aerosol (0.1 $\times$ $\mu$g $m^{-3}{}_{STP}$). Yellow indicates ethane (0.01 $\times$ ppbv). Orange indicates PAN (0.01 $\times$ ppbv).

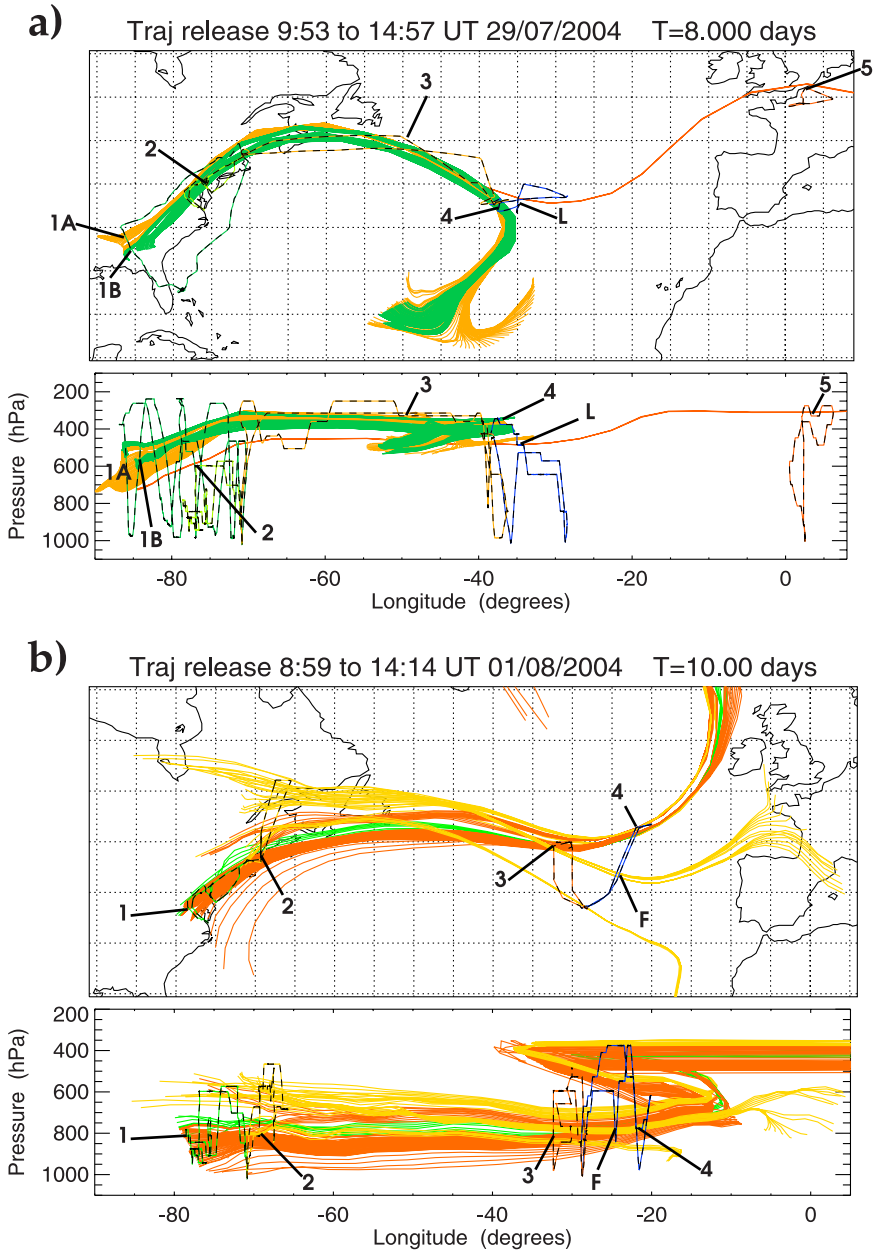


**Figure 10.** Lagrangian links between hydrocarbon samples from different flights with similar fingerprints ("coincident matches"). (a) Case 4: trajectories 4 days forward and backward from the BAe146 flight track on 29 July (blue). Matching flights are DC8 25 July (dark green), WP-3D 27 July (light green), DC8 28 July (orange) and Falcon 31 July (red), labeled in time order. L marks location of line convection. (b) Case 5: trajectories 5 days forward and backward from the BAe146 flight track on 1 August (blue). Matching flights are WP-3D 27 July (green), WP-3D 28 July (yellow), and BAe146 31 July (red). F marks interception of a fire plume.

modeled by FLEXPART and the UGAMP trajectory model, is marked "P3" on Figure 11. Clearly, it is displaced to the north relative to the BAe146 flight track and the trajectories (red in Figure 10a) pass under the flight track and just fail the trajectory match criterion. However, tracer concentrations were observed to be horizontally uniform in this area, probably because of previous mixing over the USA, making a reasonable Lagrangian match between the WP-3D and BAe146. Also, their hydrocarbon fingerprints were highly correlated.

[94] The BAe146 also has coincident matches with the DC8 on 25 and 28 July and Falcon on 31 July. On the outbound track of the BAe146 (see Figure 11), a fire plume was encountered in the cold, dry air (low $\theta_e$) at the northernmost point before turning south into the warm conveyor belt outflow at around 475 hPa. A long line of deep convection was crossed. It was observed on the aircraft navigation radar to extend at least 100 km to the east and west, although only 10 km wide with cloud tops at around 270 hPa. The best Lagrangian match with the Falcon on

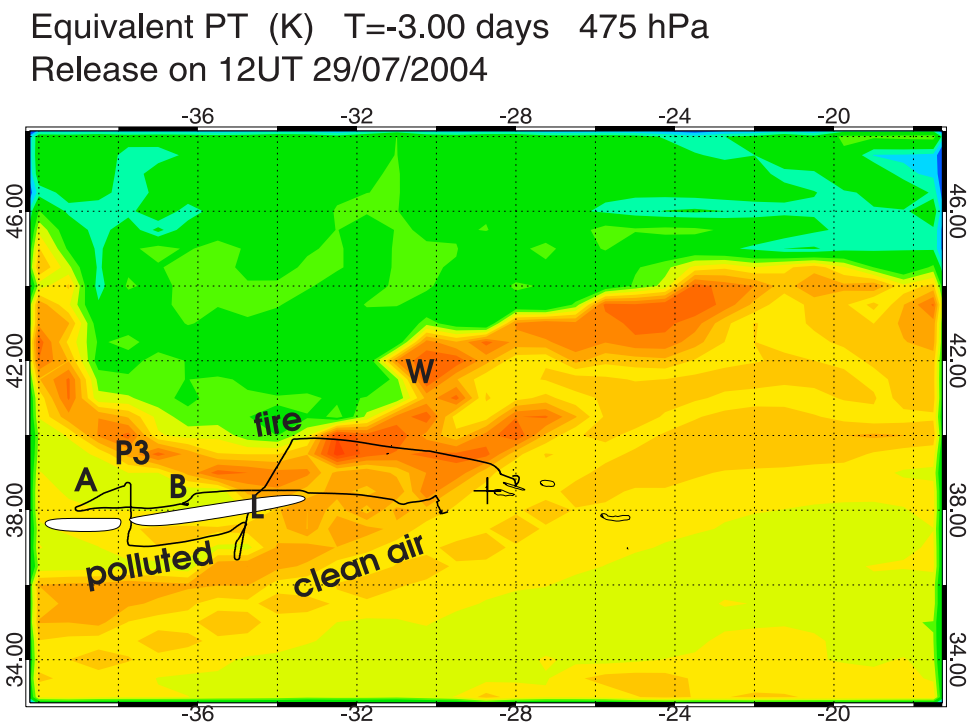


**Figure 11.** RDF3D reconstruction of $\theta_e$ on the 475 hPa surface, 1200 UT 29 July 2004. The flight track of the BAe146 is shown shifted relative to air mass locations at 1200 UT. A long line of deep convection (marked in white) was first crossed at point L. Data on the descent from A to B are shown in Figure 12. The descent was in polluted air, while models indicate that the air south of the front (yellow) was clean. W marks a weak frontal wave. Contour interval is 2.5 K, ranging from 317.5 K (blue) to 340 K (red).

31 July (red trajectories in Figure 10a) occurred here (below the main pollution). A gap in the line convection was crossed northward at 350 hPa ($\approx$ 8.1 km). The best coincident matches with the DC8 on 25 and 28 July were south of the line convection on the highest flight level (case 4A in Table 1, orange trajectories in Figure 10a) but north of the line convection with there are also coincident matches with the DC8 on 25 July (case 4B, green trajectories). *Lewis et al.* [2006, Figure 11] show a vertical section across the WCB from the RDF3D simulation which indicates that the WCB extended up to about 250 hPa, the top of the observed line convection. Simulated trajectory ascent is also stronger just to the east and south of the highest-level segment of flight track, with resolved flow trajectories extending into the continental boundary layer (unlike the match trajectories shown).

[95] Figure 12 shows the descent through the WCB from point A to 1000 feet ASL at point B. The polluted outflow layer is seen above 5 km. This layer was convectively stable ($\partial\theta_e/\partial z > 0$), enabling the persistence of layering in constituents. PAN is much higher than in the low-level case 1, while sulfate aerosol concentrations are much lower. This may be a signature of the contrast in origin with case 1 (SE USA rather than Ohio River Valley) and/or the influence of wash out on sulfate in the warm conveyor belt.

[96] Table 1 shows that $\theta$ increases by almost 20 K, associated with latent heat release, while $\theta_e$ is conserved. CO is more variable between the matching windows than within each window indicating that the Lagrangian matches are not perfect. The DC8 on 28 July and BAe146 on 29 July are most closely linked and clearly CO decreases with time over this day. PAN and ozone are indistinguishable between these match windows. Note that the DC8 on 28 July observed total PNs concentrations of 606 (64) pptv, implying that 94% of PNs was in the form of PAN. The slightly lower CO observed earlier by the DC8 on 25 July and WP-3D on 27 July may indicate simply a displacement relative to the

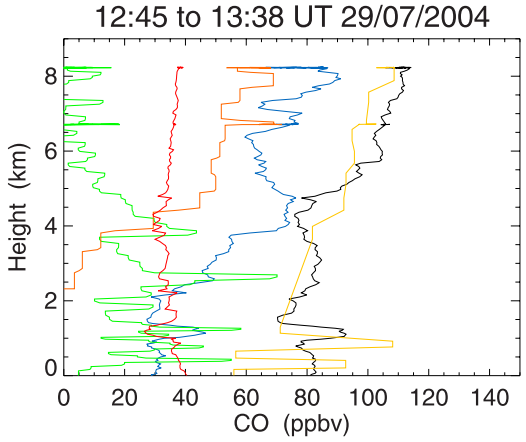


**Figure 12.** Measurements on descent through WCB outflow made by the BAe146 between 1245 and 1338 UT on 29 July 2004. Black indicates CO (ppbv). Blue indicates ozone (ppbv). Green indicates sulfate aerosol (0.01 $\times$ $\mu$g $m^{-3}{}_{STP}$). Yellow indicates ethane (0.01 $\times$ ppbv). Orange indicates PAN (0.01 $\times$ ppbv). Red indicates $\theta_e$ $-$ 300 (K).

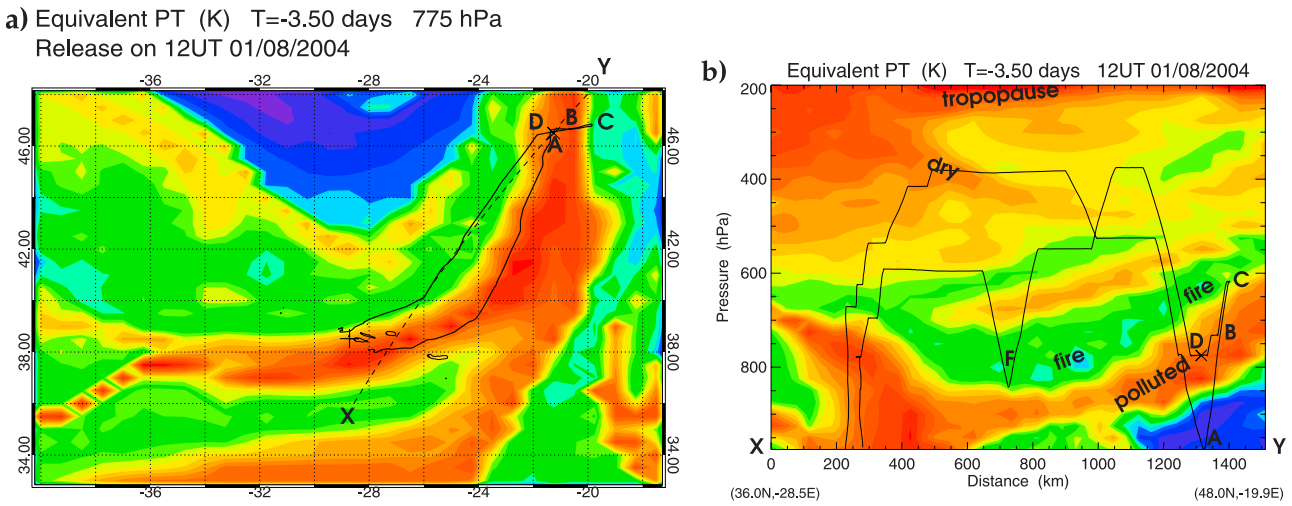


**Figure 13.** (a) RDF3D reconstruction of $\theta_e$ on the 775 hPa surface, 1200 UT 1 August 2004. The flight track of the BAe146 is shown shifted relative to air mass locations at 1200 UT. A run was made at this level through the front between points B and D. The plus symbol marks Faial. (b) Great circle cross section XY. The BAe146 flight track is projected onto the section. The cross at point D marks the case 5 Lagrangian match in the polluted air just above the $\theta_e$ maximum. Point F is a Lagrangian match with the WP-3D in a forest fire plume. Contour interval is 2.5 K, ranging from 302.5 K (indigo) to 342.5 K (red).

air mass seen by the BAe146 or mixing of further CO into the air mass after these upwind intersections. The WP-3D was flying through deep convection within the match window. Ozone was extremely uniform within each match window and increases with time following the air mass, indicative of photochemical production. PAN also increases as the air mass ascends between the 25 July and 28 July, consistent with conversion from $NO_x$. Figure 5d (red symbols) shows that the air sampled by the Falcon on 31 July had been recently influenced by fresh emissions from Europe. In addition, two spikes in NO were observed during this match window. However, the $NO_y$ is not much greater than the upstream PAN observations, consistent with a Lagrangian match and the assumption that most $NO_y$ is in the form of PAN in the upper troposphere.

#### 6.2.5. Case 5: Low-Level Export by Frontal System

[97] The air from the polluted boundary layer over the USA that did not fall within the footprint of the WCB or get lofted by convection was exported to the east by the slower winds in the lower troposphere. Warm, moist air with high $\theta_e$ from the SE USA was advected along the east coast ahead of the surface cold front picking up pollution and then out toward the Azores (red trajectories in Figure 10b). The front passed over the Azores on 1 August 2004 and the warm sector (high $\theta_e$) can be seen at 775 hPa in Figure 13a. Air on the northwestern flank of the $\theta_e$ maximum was polluted while air on the southeastern flank was cleaner because of its trajectories missing landfall over the USA. The front was forward sloping (tilts up toward the south and east, see Figure 13b).

[98] The best Lagrangian matches occurred on the polluted northwest side of the front on descent toward A, at point B on ascent and descent and then a level run to D (see Figure 13b). It can be linked to the BAe146 intersecting the front on 31 July and the WP-3D on 27 and 28 July. Figure 14 shows measurements on ascent and descent across frontal surface between points A and D. The polluted side of the front was crossed on ascent through B, descent to B and then on a slightly lower level run to D. At these locations CO, ethane and ozone are elevated relative to their surroundings, but not a great deal. Sulfate aerosol shows greater contrast with the clean side of the front, although is clearly much lower than in case 1.

[99] The top of the profile at point C is influenced by forest fire emissions into air that had descended from near tropopause level over Canada. These fire emissions were encountered wherever the flight crossed the low $\theta_e$ layer (green) in Figure 13b. The profiles down and up through the

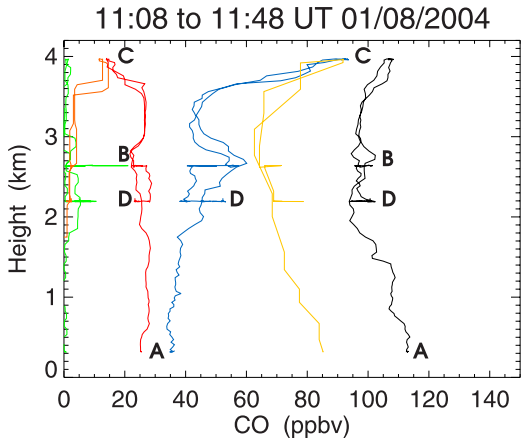


**Figure 14.** Measurements on ascent and descent across frontal surface made by the BAe146 between 1108 and 1148 UT on 1 August 2004. Black indicates CO (ppbv). Blue indicates ozone (ppbv). Green indicates sulfate aerosol ($0.1 \times \mu g\ m^{-3}{}_{STP}$). Yellow indicates ethane ($0.01 \times$ ppbv). Orange indicates PAN ($0.01 \times$ ppbv). Red indicates $\theta_e - 300$ (K). Points A, B, C and D along the track are marked. The case 5 Lagrangian match is on the level run to point D.

fire layer near F revealed that CO was highest near the bottom of the layer (150 ppbv) but near the top there was a dry layer with higher ozone. Very similar characteristics were observed by the BAe146 on 31 July: At this earlier time the top layer contained ozone up to 200 ppbv, implying that the fire emissions had mixed with stratospheric air. Point F also has coincident matches with the WP-3D on 28 July when it intercepted the fire plume north of the St. Lawrence River (yellow trajectories in Figure 10b).

[100] In case 5, $\theta$ decreases slowly with time and $\theta_e$ decreases at a faster rate. This could be explained by mixing between the high $\theta_e$ of the polluted air mass and the very low $\theta_e$ of the cold, dry layer immediately above the frontal surface (see Figure 13b). CO barely changes with time since the CO contrast between the two air masses is very weak (Figure 14). An increase in benzene/ethane ratio (a characteristic of fire plume case 2) between 31 July and 1 August supports the hypothesis of mixing with the fire layer. PAN decreases with time associated with thermal decomposition. Ozone decreases with time, but modeling studies are required to determine the contribution from photochemical loss.

## 7. Conclusions

[101] Evidence has been presented to demonstrate that air masses were sampled several times during transit across the North Atlantic as part of the ITCT-Lagrangian-2K4 experiment. Many Lagrangian matches were identified objectively using a novel technique that combines Lagrangian trajectories, calculated using global meteorological analyses, and the hydrocarbon fingerprints analyzed from whole air samples collected by the aircraft. Five cases were identified with strong links between at least three flights spanning the Atlantic. The variability between the hydrocarbon fingerprints of linked samples is very small compared to the differences between randomly selected samples, once the loss of hydrocarbons through OH reaction over the time between samples is accounted for. The relationships between the longer-lived hydrocarbons are particularly close, with variability comparable to the variability between samples collected on one flight through the same air mass.

[102] There is always uncertainty concerning the closeness of the Lagrangian matches. The ideal situation would be for the differences between downwind and upwind interceptions of an air mass to reveal photochemical transformation in composition. However, two factors render this task difficult:

[103] 1. Variability within an air mass, since the upwind and downwind aircraft may sample the air mass differently, even if its structure and composition had not changed over the interval between flights. For example, in case 2, following the Alaskan fire plume, there was strong variability in CO and the DC8 and BAe146 spent a different fraction of time near the CO maximum. There is also uncertainty in the vertical structure of the plume and the level of the aircraft relative to the plume maximum. However, other tracers, that are not directly emitted from the fires, are much more uniform. For example, equivalent potential temperature agrees to within 1 K between the interceptions of the DC8, BAe146 and Falcon through the plume. Since ozone variability is small within the plume it is reasonable to suggest that the downwind minus upwind differences are a good estimate of ozone evolution.

[104] 2. Mixing by turbulence following the flow resolved in atmospheric analyses. In the Lagrangian experiment, the rate of mixing was not observed between interceptions and the gradients with neighboring air masses, which change continuously, were also not sampled between flights. The only quantitative way to partition the observed change between photochemical reaction and physical processes is through the use of a model.

[105] Bearing these limitations in mind, the quality of different matching techniques was assessed using independent observations of tracers to find downwind minus upwind differences. The distribution of $\theta_e$ differences for trajectory-only or hydrocarbon-only matches was much more strongly peaked about zero than pairing random time points drawn from the same set of flights. Importantly, when the information was combined in the search for ''coincident matches'' the peak of the PDF more than doubled, showing that the quality of these matches was much higher. With the exception of the coincident trajectories in case 3, the $\theta_e$ differences almost all lie within $-3$ to $+1$ K day$^{-1}$, consistent with pseudoadiabatic evolution following air masses. Potential temperature increase shows that some of these coincident matches experienced latent heat release associated with ascent and condensation. In addition, the PDFs were very similar when using the UGAMP trajectory model or FLEXPART Lagrangian dispersion model, together with hydrocarbon fingerprints, to identify matches. This indicates that the quality of the matches identified using two different models, with different trajectory matching criteria, are similar even though there are differences in the match windows highlighted.

[106] The PDF of CO growth rate (defined by (3)) shows CO increase for a few matches, either indicating a mismatch or mixing of more CO into the air mass. However, in the vast majority of cases there is slow CO decrease with an associated timescale of greater than 10 days for 73% of matches. The CO decreases more slowly than the timescale of turbulent mixing because the targets do not have much higher CO than their surroundings (except in the Alaskan fire plume case 2).

[107] The PDF of ozone growth rate peaks at slow increase. It is not possible to quantify the proportion associated with photochemistry, as opposed to mixing, without running a photochemical model for all matches.

[108] The best five Lagrangian cases (see Table 1) cover a variety of situations. Cases 1, 3 and 5 followed anthropogenic pollution at low levels from the east coast USA right across the Atlantic. Case 3 was clearly influenced by entrainment from a dry layer overlying the pollution (top at 850 hPa). Nevertheless, mixing was so slow that layering and strong variability in CO was still observed by the Falcon just west of Ireland. Case 1 also retained a highly stratified structure with weak mixing and virtually no shear in the flow. Two distinct air masses were identified traveling one above the other, both characterized by very high sulfate aerosol concentrations. The upper layer (1A) traveled just above the marine boundary layer and appeared to mix very slowly with its neighbors, while the lower layer (1B) descended slowly into the marine boundary layer. Continuous, but slow, entrainment from the polluted low-level

outflow helped to maintain high pollutant levels (e.g., sulfate aerosol) in the marine BL below, as observed in Lagrangian case 3 of ACE-2 [*Wood et al.*, 2000]. Ozone decrease occurred in air masses traveling at low level, even if well above the boundary layer (e.g., case 5 following a cold front). Case 2 followed a highly polluted plume originating from fires in Alaska as it descended from the upper troposphere across the Atlantic. Case 4 followed air ascending from southeast USA in a warm conveyor belt and then across the Atlantic in the upper troposphere. Ozone increase occurs in the upper troposphere in anthropogenic pollution and the Alaskan fire plume.

[109] The cases detailed in this paper provide a basis for detailed chemical transport modeling studies constrained by observations. It is hoped that changes in concentrations of compounds that are not routinely observed, such as higher hydrocarbons, OVOCs, alkyl nitrates and peroxy nitrates will reveal exciting new information about photochemical reaction pathways.

[110] **Acknowledgments.** Thanks to the whole of the ICARTT team: the scientists, pilots and support staff associated with all the measurement platforms and their campaign bases. The Natural Environment Research Council (NERC) funded the ITOP-UK project and flying time as part of the Upper Troposphere–Lower Stratosphere Ozone (UTLS) thematic programme. The ITOP-UK team would also like to give heartfelt thanks to the dedication of the staff from the Facility for Airborne Atmospheric Measurements and in particular, John Reid, without whom the BAe146 would never have reached the Azores, let alone made measurements, on its first deployment. The deployment of the DLR Falcon in Creil, France, was funded by DLR. French participation in European ITOP was funded by Programme National de Chimie Atmosphérique (PNCA) (ADEME, Agence gouvernementale de l'Environnement et de la Maitrise de l'énergie)/ PATOM (Programme Atmosphère et Océan Multi-échelles) of INSU (Institut National des Sciences de l'Univers) and IPSL (Institut Pierre Simon Laplace). Local support from IGN (Institut Géographique National), Creil, is gratefully acknowledged. Particular thanks to Tom B. Ryerson and Gerd Hübler (NOAA Earth System Research Lab) for the WP-3D core measurements, Glen W. Sachse (NASA Langley RC) for the DC8 CO measurements and Ron C. Cohen (UCI) for the DC8 total peroxynitrate measurements. John Methven is grateful for support through an Advanced Fellowship jointly sponsored by NERC and the Environment Agency.

## References

Bates, T., B. Huebert, J. Gras, F. Griffiths, and P. Durkee (1998), International Global Atmospheric Chemistry (IGAC) Project's first Aerosol Characterisation Experiment (ACE-1): Overview, *J. Geophys. Res.*, *103*, 16,297–16,318.

Day, D. A., P. J. Wooldridge, M. B. Dillon, J. A. Thornton, and R. C. Cohen (2002), A thermal dissociation laser-induced fluorescence instrument for in situ detection of $NO_2$, peroxy nitrates, alkyl nitrates, and $HNO_3$, *J. Geophys. Res.*, *107*(D6), 4046, doi:10.1029/2001JD000779.

Derwent, R., P. Simmonds, S. Seuring, and C. Dimmer (1998), Observation and interpretation of the seasonal cycles in the surface concentrations of ozone and carbon monoxide at Mace Head, Ireland from 1990 to 1994, *Atmos. Environ.*, *32*, 145–157.

Eckhardt, S., A. Stohl, H. Wernli, P. James, C. Forster, and N. Spichtinger (2004), A 15-year climatology of warm conveyor belts, *J. Clim.*, *17*, 218–237.

Esler, J., G. Roelofs, M. Köhler, and F. O'Connor (2004), A quantitative analysis of grid-related systematic errors in oxidising capacity and ozone production rates in chemistry transport models, *Atmos. Chem. Phys.*, *4*, 1781–1795.

Fehsenfeld, F., et al. (2006), International Consortium for Atmospheric Research on Transport and Transformation (ICARTT): North America to Europe: Overview of the 2004 summer field study, *J. Geophys. Res.*, doi:10.1029/2006JD007829, in press.

Fitzgerald, J., J. Marti, W. Hoppel, G. Frick, and F. Gelbard (1998), A one-dimensional sectional model to simulate multicomponent aerosol dynamics in the marine boundary layer: 2. Model application, *J. Geophys. Res.*, *103*, 16,103–16,117.

Forster, C., et al. (2001), Transport of boreal forest fire emissions from Canada to Europe, *J. Geophys. Res.*, *106*, 22,887–22,906.

Frost, G. J., et al. (2006), Effects of changing power plant NOx emissions on ozone in the eastern United States: Proof of concept, *J. Geophys. Res.*, *111*, D12306, doi:10.1029/2005JD006354.

Guenther, A., et al. (1995), A global model of natural volatile organic compound emissions, *J. Geophys. Res.*, *100*, 8873–8892.

Haynes, P., and J. Anglade (1997), The vertical-scale cascade in atmospheric tracers due to large-scale differential advection, *J. Atmos. Sci.*, *54*, 1121–1136.

Hoell, C., C. O'Dowd, S. Osborne, and D. Johnson (2000), Time-scale analysis of marine boundary layer aerosol evolution: Lagrangian case studies under clean and polluted cloudy conditions, *Tellus, Ser. B*, *52*, 423–438.

Huebert, B., A. Pszenny, and B. Blomquist (1996), The ASTEX/MAGE experiment, *J. Geophys. Res.*, *101*, 4319–4329.

Jobson, B., D. Parrish, P. Goldan, W. Kuster, F. Fehsenfeld, D. Blake, N. Blake, and H. Niki (1998), Spatial and temporal variability of nonmethane hydrocarbon mixing ratios and their relation to photochemical lifetime, *J. Geophys. Res.*, *103*, 13,557–13,567.

Johnson, D., S. Osborne, R. Wood, K. Suhre, R. Johnson, and S. Businger (2000), An overview of the Lagrangian experiments undertaken during the North Atlantic regional Aerosol Characterization Experiment (ACE-2), *Tellus, Ser. B*, *52*, 290–320.

Legras, B., B. Joseph, and F. Lefvre (2003), Vertical diffusivity in the lower stratosphere from Lagrangian back-trajectory reconstructions of ozone profiles, *J. Geophys. Res.*, *108*(D18), 4562, doi:10.1029/2002JD003045.

Lehmann, R., P. von der Gathen, M. Rex, and M. Streibel (2005), Statistical analysis of the precision of the Match method, *Atmos. Chem. Phys.*, *5*, 2713–2727.

Lewis, A., et al. (2006), Chemical composition observed over the mid-Atlantic and the detection of pollution signatures far from source regions, *J. Geophys. Res.*, doi:10.1029/2006JD007584, in press.

Methven, J. (1997), Offline trajectories: Calculation and accuracy, *Tech. Rep. 44*, U. K. Univ. Global Atmos. Modell. Program, Dep. of Meteorol., Univ. of Reading, Reading, U. K.

Methven, J., and B. Hoskins (1999), The advection of high resolution tracers by low resolution winds, *J. Atmos. Sci.*, *56*, 3262–3285.

Methven, J., S. Arnold, F. O'Connor, H. Barjat, K. Dewey, J. Kent, and N. Brough (2003), Estimating photochemically produced ozone throughout a domain using flight data and a Lagrangian model, *J. Geophys. Res.*, *108*(D9), 4271, doi:10.1029/2002JD002955.

Olivier, J., A. Bouwman, J. Berdowski, C. Veldt, J. Bloos, A. Visschedijk, C. van der Maas, and P. Zandveld (1999), Sectoral emission inventories of greenhouse gases for 1 990 on a per country basis as well as on $1 \times 1$ degree, *Environ. Sci. Policy*, *2*, 241–264.

Parrish, D. (2006), The effects of mixing on evolution of hydrocarbon ratios in the troposphere, *J. Geophys. Res.*, doi:10.1029/2006JD007583, in press.

Parrish, D., M. Trainer, J. Holloway, J. Yee, M. Warshawsky, F. Fehsenfeld, G. Forbes, and J. Moody (1998), Relationships between ozone and carbon monoxide at surface sites in the North Atlantic region, *J. Geophys. Res.*, *103*(D11), 13,357–13,376.

Pfister, G., P. Hess, L. Emmons, J.-F. Lamarque, C. Wiedinmyer, D. Edwards, G. Petron, J. Gille, and G. Sachse (2005), Quantifying CO emissions from the 2004 Alaskan wildfires using MOPITT CO data, *Geophys. Res. Lett.*, *32*, L11809, doi:10.1029/2005GL022995.

Prinn, R., R. Weiss, B. Miller, J. Huang, F. Alyea, D. Cunnold, P. Fraser, D. Hartley, and P. Simmonds (1995), Atmospheric trends and lifetime of $CH_3CCl_3$ and global OH concentrations, *Science*, *269*, 187–192.

Raes, F., T. Bates, F. McGovern, and M. van Leide (2000), The second Aerosol Characterisation Experiment (ACE-2): General overview and main results, *Tellus, Ser. B*, *52*, 111–125.

Real, E., et al. (2006), Processes influencing ozone levels in Alaskan forest fires plumes during long-range transport over the North Atlantic, *J. Geophys. Res.*, doi:10.1029/2006JD007576, in press.

Rex, M., et al. (1998), In situ measurements of stratospheric ozone depletion rates in the Arctic winter 1991/ 1992: A Lagrangian approach, *J. Geophys. Res.*, *103*(D5), 5843–5854.

Riddle, E., P. Voss, A. Stohl, D. Holcomb, D. Mazcka, K. Washburn, and R. Talbot (2006), Trajectory model validation during the International Consortium for Atmospheric Research on Transport and Transformations 2004 using newly developed altitude-controlled meteorological balloons, *J. Geophys. Res.*, *111*, D23S57, doi:10.1029/2006JD007456.

Stohl, A., S. Eckhardt, C. Forster, P. James, N. Spichtinger, and P. Seibert (2002), A replacement for simple back trajectory calculations in the interpretation of atmospheric trace substance measurements, *Atmos. Environ.*, *36*, 4635–4648.

Stohl, A., et al. (2003), A backward modeling study of intercontinental pollution transport using aircraft measurements, *J. Geophys. Res.*, *108*(D12), 4370, doi:10.1029/2002JD002862.

Stohl, A., O. Cooper, R. Damoah, F. Fehsenfeld, C. Forster, E.-Y. Hsie, G. Hübler, D. Parrish, and M. Trainer (2004), Forecasting for a Lagrangian aircraft campaign, *Atmos. Chem. Phys.*, *4*, 1113–1124.

Stohl, A., C. Forster, A. Frank, P. Seibert, and G. Wotawa (2005), The Lagrangian particle dispersion model FLEXPART version 6.2, *Atmos. Chem. Phys.*, *5*, 2461–2474.

Wood, R., et al. (2000), Boundary layer and aerosol evolution during the 3rd Lagrangian experiment of ACE-2, *Tellus, Ser. B*, *52*, 401–422.

S. R. Arnold, M. J. Evans, and J. McQuaid, School of Earth and Environment, University of Leeds, Leeds LS2 9JT, UK.

E. Atlas, Rosenstiel School of Marine and Atmospheric Science, University of Miami, Miami, FL 33149-1098, USA.

M. Avery, NASA Langley Research Center, Hampton, VA 23681, USA.

D. R. Blake, Department of Chemistry, University of California, Irvine, CA 92697, USA.

H. Coe, J. Crosier, and P. I. Williams, School of Earth, Atmospheric and Environmental Sciences, University of Manchester, Manchester M13 9PL, UK.

F. M. Flocke, Atmospheric Chemistry Division, National Center for Atmospheric Research, Boulder, CO 80305, USA.

J. S. Holloway and D. D. Parrish, Earth System Research Laboratory, NOAA, Boulder, CO 80305, USA.

J. R. Hopkins, A. C. Lewis, and N. M. Watson, Department of Chemistry, University of York, York YO10 5DD, UK.

K. Law, Service d'Aéronomie, Centre National de la Recherche Scientifique, Université Pierre et Marie Curie, F-75252 Paris, France.

J. Methven, Department of Meteorology, University of Reading, P.O. Box 243, Earley Gate, Reading RG6 6BB, UK. (j.methven@reading.ac.uk)

P. S. Monks, Department of Chemistry, University of Leicester, Leicester LE1 7RH, UK.

R. Purvis, Facility for Airborne Atmospheric Measurements, Cranfield MK43 0AL, UK.

B. Rappenglück, Institute of Meteorology and Climate Research, Forschungszentrum Karlsruhe, D-82467 Garmisch-Partenkirchen, Germany.

C. E. Reeves, School of Environmental Sciences, University of East Anglia, Norwich NR4 7TJ, UK.

H. Schlager, Deutsches Zentrum für Luft- und Raumfahrt, D-82230 Oberpfaffenhofen, Germany.

H. B. Singh, NASA Ames Research Center, Moffett Field, CA 94035, USA.

A. Stohl, Norwegian Institute for Air Research, N-2027 Kjeller, Norway.

L. K. Whalley, School of Chemistry, University of Leeds, Leeds LS2 9JT, UK.